We are IntechOpen,
the world's leading publisher of
Open Access books
Built by scientists, for scientists

4,800
Open access books available

122,000
International authors and editors

135M
Downloads

Our authors are among the

154
Countries delivered to

TOP 1%
most cited scientists

12.2%
Contributors from top 500 universities

CLARIVATE ANALYTICS
BOOK CITATION INDEX
INDEXED

WEB OF SCIENCE™

Selection of our books indexed in the Book Citation Index
in Web of Science™ Core Collection (BKCI)

Interested in publishing with us?
Contact book.department@intechopen.com

Energy Transfer in Mixed Convection MHD Flow of Nanofluid Containing Different Shapes of Nanoparticles in a Channel Filled with Saturated Porous Medium

Aaiza Gul, Ilyas Khan and Sharidan Shafie

Additional information is available at the end of the chapter

Abstract

Energy transfer in mixed convection unsteady magnetohydrodynamic (MHD) flow of an incompressible nanofluid inside a channel filled with a saturated porous medium is investigated. The walls of the channel are kept at constant temperature, and uniform magnetic field is applied perpendicular to the direction of the flow. Three different flow situations are discussed on the basis of physical boundary conditions. The problem is first written in terms of partial differential equations (PDEs), then reduces to ordinary differential equations (ODEs) by using a perturbation technique and solved for solutions of velocity and temperature. Four different shapes of nanoparticles inside ethylene glycol ($C_2H_6O_2$) and water (H_2O)-based nanofluids are used in equal volume fraction. The solutions of velocity and temperature are plotted graphically, and the physical behavior of the problem is discussed for different flow parameters. It is evaluated from this problem that viscosity and thermal conductivity are the dominant parameters responsible for different consequences of motion and temperature of nanofluids. Due to greater viscosity and thermal conductivity, $C_2H_6O_2$-based nanofluid is regarded as better convectional base fluid assimilated to H_2O.

Keywords: mixed convection, nanofluid, heat transfer, cylindrical-shaped nanoparticles, MHD flow, porous medium, analytical solutions

1. Introduction

1.1. Nanofluids

Thermal conductivity is the important thermophysical property that plays an essential role in heat transfer enhancement. The internal property of the material is depended on the nature of

the fluids. Changing the nature of the fluids or materials can also be affected. In contrast, by applying external force, thermal convection can also be affected on the fluids. Thermal convections are depended on the nature of the fluids as well as on the fluid flow, fluid regime, geometry, etc. Heat transfer conventional fluids, such as ethylene glycol (EG), water, and oils, which are lubricant and kerosene oil have poor thermal conductivities compared to solids. On the other hand, solid particles exhibited rich thermal conductivities than those of conventional heat transfer fluids. The significant improvements in the thermal conductivity of the fluids, which are conventional base by adding up the nanosized particles, were considered by Choi [1] for the first time. The mixture of nanosized particles containing conventional-based fluids is usually known as nanofluids. More accurately, nanofluids are suspensions of nanosized particles in base fluids. The most ordinary nanoparticles used in nanofluids are oxides, carbides, and metals. Nanofluids are mainly used in electronic equipment, power generation, energy supply, production, and air conditioning. Vajjha and Das [2] investigated, for the first time, EG (60%) and water (40%) mixture that is a base fluid for the preparation of alumina (Al_2O_3), copper oxide (CuO), and zinc oxide (ZnO) nanofluids. At the equal temperature and concentration, CuO nanofluids have higher thermal conductivity than those of Al_2O_3 and ZnO nanofluids. Naik and Sundar [3] have prepared (CuO) nanofluids with 70% propylene glycol and 30% water. As estimated, they found that CuO nanofluids have rich thermal conductivity and viscosity as compared to the other fluids that are base. Recently, Mansur et al. [4] have studied magnetohydrodynamic (MHD) stagnation-point flow of nanofluids over a permeable sheet for stretching and shrinking cases. They used bvp4c program in MATLAB to obtain the numerical solutions and computed results for different parameters.

The quality of nanofluids in terms of heat transfer performance depends on the volume fraction and types of nanoparticles as well as also depends on the shapes of nanoparticles. Many researchers have used nanoparticles in spherical shapes. However, the nanofluids containing nonspherical shapes of nanoparticles have higher thermal conductivities as compared to spherical ones. Hence, nonspherical shapes of nanoparticles are most suitable to be used. Nanoparticles other than spherical shapes have been used in this research due to their above-mentioned properties. More closely, in this study we discuss four different types of nanoparticles, namely, cylinder, platelet, blade, and brick. Nanoparticles of nonspherical shapes with desirable properties are the main focus of present study. Recently, the development in the field of nanotechnology has shown that cylindrical-shaped nanoparticles are seven times more harmful than spherical-shaped nanoparticles in the deliverance of drugs to breast cancer. In the literature survey of nanofluids, we found that analytical studies for the suspension of a variety of shapes of nanoparticles containing EG and water-based fluids are not described yet. Although Timofeeva et al. [5] study the problem of Al_2O_3 nanofluids which are of different shaped nanoparticles, but they performed experimentally with theoretical modeling together in this study. More closely, they studied various shapes of Al_2O_3 nanoparticles in a base fluid mixture of EG and water of similar volumes. Improvement in the effective thermal conductivities due to particle shapes was mentioned by Timofeeva et al. Loganathan et al. [6] considered nanoparticles that are sphere shaped and analyzed radiation effects on an unsteady natural convection flow of nanofluids over an infinite vertical plate. They have found that the velocity of spherical silver (Ag) nanofluids is less than that of copper (Cu), titanium dioxide (TiO_2), and Al_2O_3 spherical nanofluids. Recently, Asma et al.

[7] found exact solutions for free-convection flow of nanofluids at ramped wall temperature by using five various kinds of spherical-shaped nanoparticles.

Sebdani et al. [8] studied heat transfer of Al_2O_3 water nanofluid in mixed convection flow inside a square cavity. Fan et al. [9] described mixed convection heat transfer in a horizontal channel filled with nanofluids. Tiwari and Das [10] and Sheikhzadeh et al. [11] investigated laminar mixed convection flow of a nanofluid in two-sided lid-driven enclosures. Furthermore, a magnetic field in nanofluids has diverse applications such as in the metallurgy and polymer industry where hydromagnetic techniques are used. Nadeem and Saleem [12] presented the unsteady flow of a rotating MHD nanofluid in a rotating cone in the presence of magnetic field. Al-Salem et al. [13] examined MHD mixed convection flow in a linearly heated cavity. The effects of variable viscosity and variable thermal conductivity on the MHD flow and heat transfer over a nonlinear stretching sheet was studied by Prasad et al. [14]. The problem of Darcy Forchheimer mixed convection heat and mass transfer in fluid-saturated porous media in the presence of thermophoresis was discussed by Rami et al. [15]. The effect of radiation and magnetic fields on the mixed convection stagnation-point flow over a vertical stretching sheet in a porous medium bounded by a stretching vertical plate was analyzed by Hayat et al. [16]. Some other studies on mixed convection flow of nanofluids are mentioned in Refs. [17–28]. Nanofluids due to the higher conduction or heat transfer rate of together with other several applications in the field of nanoscience have attracted the attention of researchers to perform future research. Altogether, several researchers are working experimentally, some of them are using numerical simulation. However, very limited research studies are obtainable on analytical side. Experimental research mainly focuses on the enhancement of heat transfer rate of nanofluids through thermal conduction. And this study also includes heat transfer through mixed convection. Several other efforts made on nanofluids are presented in Refs. [29–39].

In order to encounter the importance of MHD in nanofluids, Mansur et al. [4] explored the MHD stagnation point flow of nanofluids over a stretching/shrinking sheet with suction. Colla et al. [21] conducted water-based nanofluids characterization, thermal conductivity and viscosity measurements, and correlation. Abareshi et al. [40] investigated fabrication, characterization, and measurement of thermal conductivity of nanofluids. Borglin et al. [41] examined experimentally the flow of magnetic nanofluids in porous media. MHD effect on nanofluid with energy and hydrothermal behavior between two collateral plates was presented by Sheikholeslami et al. [42]. Sheikholeslami et al. [43] studied forced convection heat transfer in a semiannulus under the influence of a variable magnetic field. Some other research studies on electrically conducting nanofluids are mentioned in Refs. [44–50].

In view of the above literature, the existing research is concerned with the radiative heat transfer in mixed convection MHD flow of different shapes of Al_2O_3 in EG base nanofluid in a channel filled with saturated porous medium. The foremost focus of this study is the importance of cylindrical-shaped nanofluids on several flow parameters. The uniform constant magnetic field is applied at 90° to the flow and the nanofluids are supposed electrically conducting. No slip condition is taken at the boundary walls of the channel. Three different flow cases on the basis of appropriate boundary conditions are explored. Both of the boundary walls of the channel are at rest in the first case, while motion in the fluids is induced due to

buoyancy force and external pressure gradient. In the second case, the right wall of the channel is oscillating in its own plane whereas in the third case, both of the bounding walls of the channel are set into oscillatory motions. The analytical solutions of velocity and temperature are obtained by using a perturbation technique. Graphs are plotted, and the physical behavior of the problem is discussed for different parameters of interest. Nusselt number and skin friction are also computed.

2. Derivation and solutions of governing equations

Consider flow in oscillating form of an incompressible nanofluid inside vertical porous channel. Flow of the nanofluids is supposed electrically conducting under the influence of uniform constant magnetic field. The uniform magnetic field is applied perpendicular to the direction of the flow. Reynolds number is supposed small to ignore the effect of evoked magnetic field. The external electric and electric fields due to polarization of charges are taken zero in order to ignore the influence of electric force in Lorentz force. It is assumed that at time $t = 0$, the flow is at constant temperature θ_0. Right boundary of the channel $(y = d)$ is maintained at constant temperature θ_{wR}, while the left boundary $(y = 0)$ has a uniform temperature θ_{wL}. Coordinate axis is considered where flow of fluids is moving in the x-axis direction, while the y-axis is taken perpendicular to the velocity of the flow direction.

After derivation of governing equations for quantity of motion and energy under the assumption of Boussinesq approximation are as follow:

$$\rho_{nf} \frac{\partial u}{\partial t} = -\frac{\partial p}{\partial x} + \mu_{nf} \frac{\partial^2 u}{\partial y^2} - \left(\sigma_{nf} B_0^2 + \frac{\mu_{nf}}{\kappa_1} \right) u + (\rho\beta)_{nf} \, g(\theta - \theta_0), \tag{1}$$

$$(\rho c_p)_{nf} \frac{\partial \theta}{\partial t} = \kappa_{nf} \frac{\partial^2 \theta}{\partial y^2} - \frac{\partial q}{\partial y}, \tag{2}$$

where $u = u(y, t)$, $\theta = \theta(y, t)$, ρ_{nf}, μ_{nf}, σ_{nf}, $\kappa_1 > 0$, $(\rho\beta)_{nf}$, g, $(\rho c_p)_{nf}$, κ_{nf} q specify the fluid velocity, temperature, density, dynamic viscosity, electrical conductivity, permeability of the porous medium, thermal expansion coefficient, gravitational acceleration, heat capacitance, thermal conductivity of nanofluids, and radiative heat flux in the x-direction. $-\partial p/\partial x = \lambda \exp{(i\omega t)}$ represents the pressure gradient of the flow in oscillatory form where ω is the oscillation parameter and λ is the amplitude of oscillation.

The Hamilton and Crosser [17] model for thermal conductivity and the Timofeeva et al. [5] model for calculating dynamic viscosity of nanofluids are used in order to encounter spherical and other than spherical shapes of nanoparticles inside nanofluids. From these models:

$$\mu_{nf} = \mu_f (1 + a\phi + \phi^2 b), \tag{3}$$

$$\frac{\kappa_{nf}}{\kappa_f} = \frac{\kappa_s + (m-1)\kappa_f + (n-1)(\kappa_s - \kappa_s)\phi}{\kappa_s + (m-1)\kappa_f - (\kappa_s - \kappa_f)\phi}, \tag{4}$$

where κ_f and κ_s are the thermal conductivities of the base fluid and solid nanoparticles,

respectively. The density ρ_{nf}, thermal expansion coefficient $(\rho\beta)_{nf}$, heat capacitance $(\rho c_p)_{nf}$ and thermal conductivity σ_{nf}, of nanofluids are derived by using the relations given by [6, 7]

$$(\rho c_p)_{nf} = (1 - \phi)(\rho c_p)_f + \phi(\rho c_p)_s, \rho_{nf} = (1 - \phi)\rho_f + \phi\rho_s,$$

$$(\rho\beta)_{nf} = (1 - \phi)(\rho\beta)_f + \phi(\rho\beta)_s, \kappa_{nf} = \alpha_{nf}(\rho c_p)_{nf},$$

$$\sigma_{nf} = \sigma_f \left[1 + \frac{3(\sigma - 1)\phi}{(\sigma + 2) - (\sigma - 1)\phi} \right], \sigma = \frac{\sigma_s}{\sigma_f}, \tag{5}$$

where ϕ is the volume fraction of the nanoparticles, ρ_f and ρ_s are the density of the base fluid and solid nanoparticles, respectively, μ_f is the dynamic viscosity of the base fluid, $(c_p)_f$ and $(c_p)_s$ denote the specific heat at constant pressure corresponding to the base fluid and solid nanoparticles and σ_f and σ_s are electrical conductivities of base fluids and solid nanoparticles. The total term (ρc_p) is known as heat capacitance.

Here a and b are shape constants and different for different shape of nanoparticles as presented in **Table 1** [5], μ_f, κ_f, and κ_s are the dynamic viscosity, thermal conductivity of the base fluid, and thermal conductivity of solid nanoparticles, respectively. The empirical shape factor n defined in Eq. (4) is equal to $n = 3/\Psi$, where Ψ is the sphericity. Sphericity given in Hamilton and Crosser model is the ratio of surface area of the sphere to the surface area of real particle with equal volumes. The values of sphericity for different shapes of nanoparticles are given in **Table 2** [5].

Model	Platelet	Blade	Cylinder	Brick
a	37.1	14.6	13.5	1.9
b	612.6	123.3	904.4	471.4

Table 1. Constants a and b empirical shape factors.

Model	Platelet	Blade	Cylinder	Brick
Ψ	0.52	0.36	0.62	0.81

Table 2. Sphericity Ψ for different shapes nanoparticles.

In Eqs. (1) and (2), the $(\rho c_p)_{nf}$, ρ_{nf}, $(\rho\beta)_{nf}$, κ_{nf}, and σ_{nf} of nanofluids are used from the relations given by Asma et al. [7], as

The temperature θ_0 and θ_w of both walls of the channel is assumed high and both walls are emitting radiations [20]. Therefore, radiative heat flux as a function of temperature is given by

$$-\frac{\partial q}{\partial y} = 4\alpha_0^2(\theta - \theta_0), \tag{6}$$

where α_0 is the radiation absorption coefficient.

Using Eq. (6) into Eq. (2) gives

$$(\rho c_p)_{\text{nf}} \frac{\partial \theta}{\partial t} = \kappa_{\text{nf}} \frac{\partial^2 \theta}{\partial y^2} - 4\alpha_0^2(\theta - \theta_0), \tag{7}$$

In order to convert dimensional partial differential equations (PDEs) into dimensionless PDEs, the following nondimensional variable are introduced

$$x^* = \frac{x}{d}, \ y^* = \frac{y}{d}, \ u^* = \frac{u}{U_0}, \ t^* = \frac{tU_0}{d}, \ \theta^* = \frac{\theta - \theta_0}{\theta_w - \theta_0}, \\ p^* = \frac{d}{\mu U_0}p, \ \omega^* = \frac{d\omega_1}{U_0}, \tag{8}$$

After dimensionalization (dropping for convenience) Eqs. (1) and (7) give

$$\left[(1 - \phi) + \phi\frac{\rho_s}{\rho_f}\right]\text{Re}\frac{\partial u}{\partial t} = \lambda \exp(i\omega t) + (1 + a\phi + b\phi^2)\frac{\partial^2 u}{\partial y^2} - \\ \left[1 + \frac{3(\sigma - 1)\phi}{(\sigma + 2) - (\sigma - 1)\phi}\right]M^2 u - \frac{1}{K}(1 + a\phi + b\phi^2) + \left[(1 - \phi) + \frac{\phi(\rho\beta)_s}{(\rho\beta)_f}\right]Gr\theta, \tag{9}$$

$$\frac{Pe}{\lambda_n}\left[(1 - \phi) + \phi\frac{(\rho c_p)_s}{(\rho c_p)_f}\right]\frac{\partial \theta}{\partial t} = \frac{\partial^2 \theta}{\partial y^2} + \frac{N^2}{\lambda_n}\theta, \tag{10}$$

where

$$Re = \frac{U_0 d}{v_f}, M^2 = \frac{\sigma_f B_0^2 d^2}{\mu_f}, K = \frac{\kappa_1}{d^2} Gr = \frac{g\beta_f d^2(\theta_w - \theta_0)}{v_f U_0}, \ Pe = \frac{(\rho c_p)_f dU_0}{\kappa_f}, \\ \lambda_n = \frac{\kappa_{nf}}{\kappa_f} = \frac{\kappa_s + (m - 1)\kappa_f + (n - 1)(\kappa_s - \kappa_s)\phi}{\kappa_s + (m - 1)\kappa_f - (\kappa_s - \kappa_f)\phi}, N^2 = \frac{4d^2\alpha_0^2}{\kappa_f}.$$

Here Re, M, Gr, Pe, and N denote the Reynolds number, magnetic parameter, the thermal Grashof number, the Peclet number, and the radiation parameter, respectively. Three different flow cases are considered in order to solve Eqs. (9) and (10). These are as follow:

2.1. Case I: Stationary walls of the channel

In this case, the gap between the two plates of the channel is denoted by d and both plates are assumed stationary at $y = 0$ and $y = d$. The flow of nanofluids is unidirectional and moving with velocity in the x-axis. Both plates of the channel are maintained at constant and uniform temperature θ_w and θ_0. Thus, the appropriate boundary conditions are

$$u(0, t) = 0, \ u(d, t) = 0, \tag{11}$$

$$\theta(0, t) = \theta_0, \ \theta(d, t) = \theta_w. \tag{12}$$

After reducing Eqs. (11) and (12) into dimensionless form, we get

$$u(0,\ t) = 0; \quad u(1,\ t) = 0, \quad t > 0, \tag{13}$$

$$\theta(0,\ t) = 0; \quad \theta(1,\ t) = 1; \quad t > 0. \tag{14}$$

Further simplification of Eqs. (9) and (10) after conversion of dimensional PDEs, we get

$$d_0 \frac{\partial u}{\partial t} = \lambda \exp(i\omega t) + \phi_2 \frac{\partial^2 u}{\partial y^2} - h_0^2 u + d_1 \theta, \tag{15}$$

$$e_0 \frac{\partial \theta}{\partial t} = \frac{\partial^2 \theta}{\partial y^2} + e_1 \theta, \tag{16}$$

where

$$d_0 = \phi_1 Re, \phi_1 = (1 - \phi) + \phi \frac{\rho_s}{\rho_f}, \phi_2 = (1 + a\phi + b\phi^2), h_0^2 = \phi_5 M^2 + 1/K,$$

$$\phi_5 = \left[1 + \frac{3(\sigma - 1)\phi}{(\sigma + 2) - (\sigma - 1)\phi}\right], d_1 = \phi_3 Gr, \phi_3 = (1 - \phi) + \phi \frac{(\rho\beta)_s}{(\rho\beta)_f}, e_0{}^2 = \frac{Pe\phi_4}{\lambda_n},$$

$$\phi_4 = \left[(1 - \phi) + \phi \frac{(\rho c_p)_s}{(\rho c_p)_f}\right], e_1{}^2 = \frac{N^2}{\lambda_n}.$$

Perturb-type solutions are supposed to convert PDEs in Eqs. (15) and (16) under appropriate boundary conditions, and in Eqs. (11) and (12) into ordinary differential equations (ODEs) are

$$u(y,\ t) = [u_0(y) + \varepsilon \exp(i\omega t) u_1(y)], \tag{17}$$

$$\theta(y,\ t) = [\theta_0(y) + \varepsilon \exp(i\omega t) \theta_1(y)]. \tag{18}$$

Using Eqs. (17) and (18) into Eqs. (15) and (16), we obtain the following system of ordinary differential equations

$$\frac{d^2 u_0(y)}{dy^2} - h_1^2 u_0(y) = d_2 \theta_0(y), \tag{19}$$

$$\frac{d^2 u_1(y)}{dy^2} - h_2^2 u_1(y) = -\frac{\lambda}{\phi_2}, \tag{20}$$

$$\frac{d^2 \theta_0(y)}{dy^2} - e_1^2 \theta_0(y) = 0, \tag{21}$$

$$\frac{d^2 \theta_1(y)}{dy^2} + h_3^2 \theta_1(y) = 0, \tag{22}$$

where

$$h_1 = \sqrt{\frac{h_0^2}{\phi_2}}, \quad d_2 = \frac{d_1}{\phi_2}, \quad h_2 = \sqrt{\frac{h_0^2 + i\omega d_0}{\phi_2}}, \quad h_3 = \sqrt{e_1 - i\omega e_0}.$$

The associated boundary conditions (Eqs. (13) and (14)) are reduce to

$$u_0(0) = 0; \quad u_0(1) = 0, \tag{23}$$

$$u_1(0) = 0; \quad u_1(1) = 0, \tag{24}$$

$$\theta_0(0) = 0; \quad \theta_0(1) = 1, \tag{25}$$

$$\theta_1(0) = 0; \quad \theta_1(1) = 0. \tag{26}$$

Perturb solution for temperature in Eqs. (21) and (22) under appropriate boundary conditions (Eqs. (25) and (26)) give

$$\theta_0(y) = \frac{\sin(e_1 y)}{\sin(e_1)}, \tag{27}$$

$$\theta_1(y) = 0. \tag{28}$$

Temperature of nanofluids, Eq. (18) using Eqs. (27) and (28) gives

$$\theta(y, t) = \theta(y) = \frac{\sin(e_1 y)}{\sin(e_1)}. \tag{29}$$

Perturb solution for temperature in Eqs. (19) and (20), using Eq. (27) under appropriate boundary conditions, Eqs. (23) and (24) yield

$$u_0(y) = c_1 \sinh(h_1 y) + c_2 \cosh(h_1 y) + \frac{d_2}{(e_1^2 + h_1^2)} \frac{\sin(e_1 y)}{\sin(e_1)}. \tag{30}$$

$$u_1(y) = c_3 \sinh(h_2 y) + c_4 \cosh(h_2 y) + \frac{\lambda}{h_2^2 \phi_2}. \tag{31}$$

Here $c_1, \ c_2, c_3$ and c_4 are arbitrary constants given by

$$c_1 = -\frac{d_2}{\sinh(h_1)(e_1^2 + h_1^2)}, c_2 = 0, c_3 = \frac{\lambda}{h_2^2 \phi_2} \frac{1}{\sinh(h_2)}(\cosh(h_2) - 1), c_4 = -\frac{\lambda}{h_2^2 \phi_2}. \tag{32}$$

Final velocity for nanofluids, substituting Eqs. (30)–(32) into Eq. (17), we obtain

$$u(y, \ t) = -\frac{d_2 \sinh(h_1 y)}{(e_1^2 + h_1^2)\sinh(h_1)} + \frac{d_2 \sin(e_1 y)}{(e_1^2 + h_1^2)\sin(e_1)}$$

$$+ \varepsilon \exp(i\omega t) \begin{bmatrix} \dfrac{\lambda(\cosh(h_2) - 1)\sinh(h_2 y)}{h_2^2 \phi_2 \sinh(h_2)} \\[3mm] + \dfrac{\lambda}{h_2^2 \phi_2}\left(1 - \cosh(h_2 y)\right) \end{bmatrix}. \tag{33}$$

2.2. Case 2: right plate of the channel is oscillating in its own plane

In this case, the right wall of the channel ($y = d$) is locate into oscillatory motion, while on other hand, the left wall ($y = 0$) is taken as stationary. The first boundary condition is the same, while the second boundary condition in dimensionless form modifies to

$$u(1,\ t) = H(t)\varepsilon \exp(i\omega t); \quad t > 0, \tag{34}$$

where $H(t)$ is the Heaviside step function.

By using the same procedure as in Case-1, and the velocity solution is obtained as

$$u(y,\ t) = -\frac{d_2 \sinh(h_1 y)}{\sinh(h_1)(e_1^2 + h_1^2)} + \frac{d_2}{(e_1^2 + h_1^2)} \frac{\sin(e_1 y)}{\sin(e_1)}$$

$$+ \varepsilon \exp(i\omega t) \left[\begin{array}{c} \dfrac{\sinh(h_2 y)}{\sinh(h_2)} \left(H(t) + \dfrac{\lambda}{(h_2^2 \phi_2)} \left(\cosh(h_2) - 1 \right) \right) \\[12pt] -\dfrac{\lambda}{(h_2^2 \phi_2)} \cosh(h_2 y) + \dfrac{\lambda}{(h_2^2 \phi_2)} \end{array} \right]. \tag{35}$$

2.3. Case 3: both plates of the channel are oscillating in its own plane

In this case, both plates of the channel are chosen into oscillatory motions. The dimensionless form of the boundary conditions is

$$u(0,\ t) = u(1,\ t) = H(t)\varepsilon \exp(i\omega t); \quad t > 0. \tag{36}$$

The resulting expression for velocity is obtained as

$$u(y,\ t) = -\frac{d_2 \sinh(h_1 y)}{\sinh(h_1)(e_1^2 + h_1^2)} + \frac{d_2}{(e_1^2 + h_1^2)} \frac{\sin(e_1 y)}{\sin(e_1)}$$

$$+ \varepsilon \exp(i\omega t) \left[\begin{array}{c} \dfrac{\sinh(h_2 y)}{\sinh(h_2)} \left(\begin{array}{c} H(t)\left(1 - \cosh(h_2 y) \right) + \\[6pt] \dfrac{\lambda}{(h_2^2 \phi_2)} \left(\cosh(h_2) - 1 \right) \end{array} \right) \\[18pt] + \left\{ H(t) - \dfrac{\lambda}{(h_2^2 \phi_2)} \right\} \cosh(h_2 y) + \dfrac{\lambda}{(h_2^2 \phi_2)} \end{array} \right]. \tag{37}$$

2.4. Evaluation of Nusselt number and skin-friction

The dimensionless derivations for Nusselt number and skin-frictions are evaluated from Eqs. (29), (33), (35) and (37) as follows:

$$Nu = \frac{e_1}{\sin(e_1)}, \tag{38}$$

$$\tau_1 = \tau_1(t) = -\frac{d_2 h_1}{(e_1^2 + h_1^2)\sinh(h_1)} + \frac{d_2 b_1}{(e_1^2 + h_1^2)\sin(e_1)}$$
$$+ \varepsilon \exp(i\omega t) \left[\frac{\lambda(\cosh(h_2) - 1)}{h_2 \phi_2 \sinh(h_2)} \right]. \tag{39}$$

$$\tau_2 = \tau_2(t) = -\frac{d_2 h_1}{(e_1^2 + h_1^2)\sinh(h_1)} + \frac{d_2 e_1}{(e_1^2 + h_1^2)\sin(e_1)}$$
$$+ \varepsilon \exp(i\omega t) \left[\frac{h_2}{\sinh(h_2)} \left\{ H(t) + \frac{\lambda}{(h_2 \phi_2)} \left(\cosh(h_2) - 1\right) \right\} \right], \tag{40}$$

$$\tau_3 = \tau_3(t) = -\frac{d_2 h_1}{(e_1^2 + h_1^2)\sinh(h_1)} + \frac{d_2 b_1}{(e_1^2 + h_1^2)\sin(e_1)}$$
$$+ \varepsilon \exp(i\omega t) \left[\frac{h_2}{\sinh(h_2)} \left\{ \begin{array}{c} H(t)\left(1 - \cosh(h_2)\right) \\ + \frac{\lambda}{(h_2^2 \phi_2)} \left(\cosh(h_2) - 1\right) \end{array} \right\} \right]. \tag{41}$$

3. Graphical consequences and depiction

In this segment, graphical consequences are figured and debated. Similarly, influence of the radiation effect on heat transfer in mixed convection MHD flow of nanofluids inside a channel filled with a saturated porous medium is explored. Three different flow cases on the basis of appropriate boundary conditions are examined. Four dissimilar shapes of Al_2O_3 as solid nanoparticles, which are cylinder, platelet, brick, and blade, are dangling into conventional base fluids, ethylene glycol and water. The physical performance of the exhibited graphs is conferred for various embedded parameters. The numerical values of constants a and b (called shape factors) are chosen from **Table 1**, and sphericity Ψ is given in **Table 2**. It should be acclaimed that a and b coefficients vary highly with particle shape. The numerical values for the various shapes of nanoparticles (platelet, blade, cylinder and brick) at equal volumes are presented in **Tables 1–3**.

The geometry of the problem is shown in **Figure 1**. The impact of dissimilar shapes of alumina Al_2O_3 nanoparticles on the motion of ethylene glycol-based nanofluids is represented in **Figure 2**. It is viewed that the blade shape of alumina Al_2O_3 nanoparticles inside ethylene glycol-based nanofluids has the uppermost velocity chased by brick, platelet, and cylindrical-shaped nanoparticles in ethylene glycol-based nanofluids. The impact of the shapes on the motion of nanofluids is because of the strong subjection of viscosity on particle shapes for $\phi < 0.1$. It is exonerated from the present consequences that the elongated shaped nanoparticles like cylinder and platelet have larger viscosities as assimilated to nanofluids comprising square-shaped nanoparticles like brick and blade. The acquired consequences

agree well with the experimental consequences predicted by Timofeeva et al.. A very small divergence is perceived in the present research, where the cylindrical-shaped nanoparticles have the larger viscosity, whereas from the experimental findings perceived by Timofeeva et al., the platelet has the larger viscosity. Timofeeva et al. had assimilated their consequences with the Hamilton and Crosser model and found that their consequences were equivalent with the Hamilton and Crosser model. In the current work, the model of Hamilton and Crosser is applied and found that analytical consequences in this research also identical to the experimental consequences of Timofeeva et al.

Model	$\rho(Kgm^{-3})$	$c_P(kg^{-1}K^{-1})$	$k(Wm^{-1}K^{-1})$	$\beta \times 10^{-5}(K^{-1})$	σ (s/m)
H_2O	997.1	4179	0.613	21	5.5×10^{-6}
$C_2H_6O_2$	1.115	0.58	0.1490	6.5	1.07×10^{-6}
Cu	8933	385	401	1.67	59.6×10^6
TiO_2	4250	686.2	8.9528	0.9	2.6×10^6
Ag	10,500	235	429	1.89	6.30×10^7
Al_2O_3	3970	765	40	0.85	$1.07 \times 10_{-6}$
Fe_3O_4	5180	670	9.7	0.5	12.7

Table 3. Thermophysical properties of water and nanoparticles.
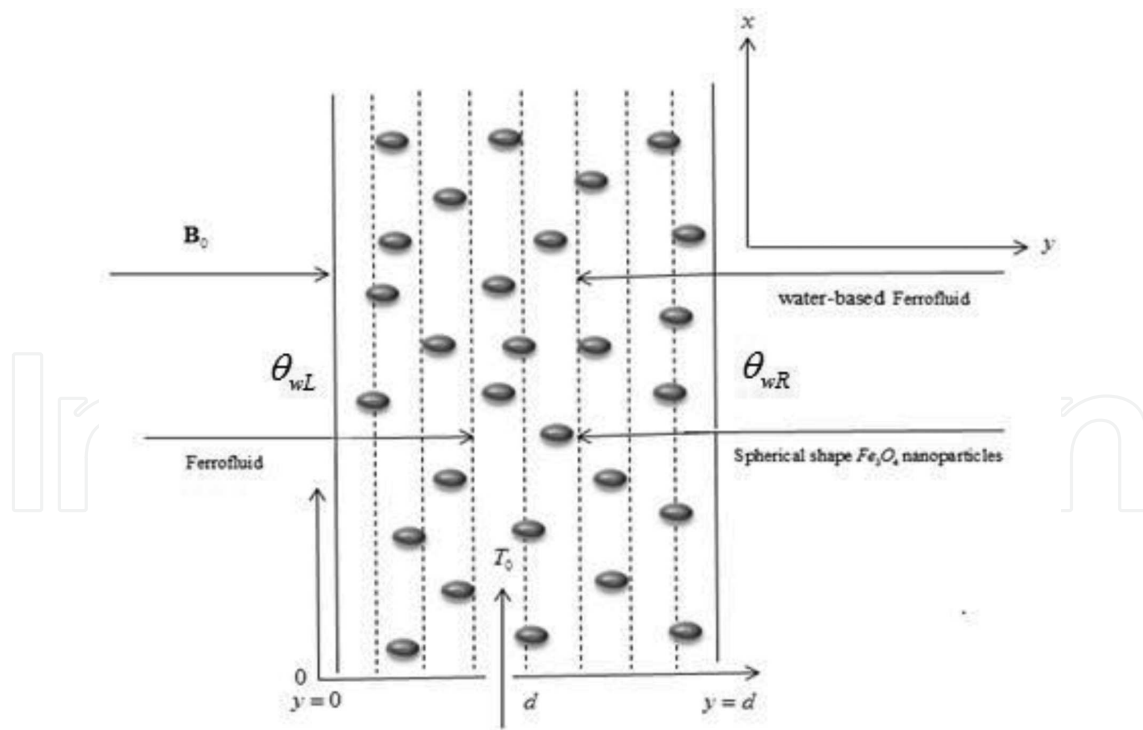
Figure 1. Physical model and coordinates system.

Figure 3 shows the result of dissimilar shapes of alumina Al_2O_3 nanoparticles on the motion of water H_2O-based nanofluids. It is surely noticed that the cylindrical-shaped alumina Al_2O_3
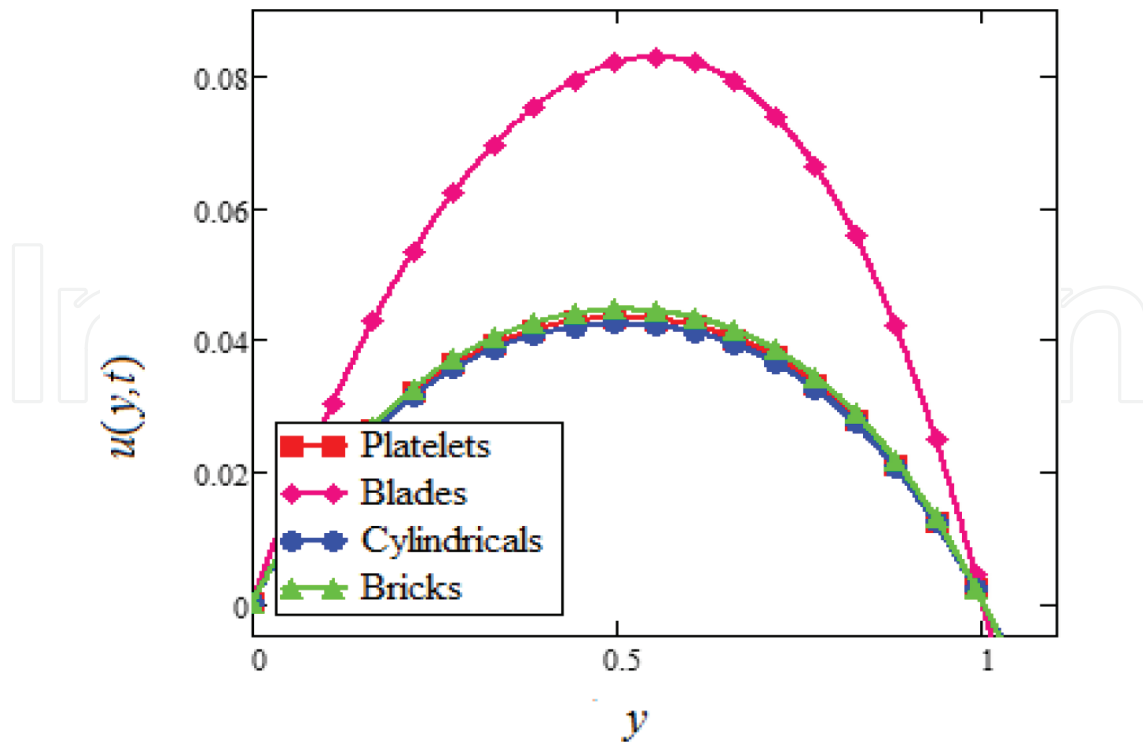
Figure 2. Velocity profiles for different shapes of Al_2O_3 nanoparticles in EG-based nanofluids when $Gr = 0.1$, $N = 0.1$, $M = 1$, $\lambda = 1$, $K = 1$, $t = 5$, $\phi = 0.04$, $\omega = 0.2$.
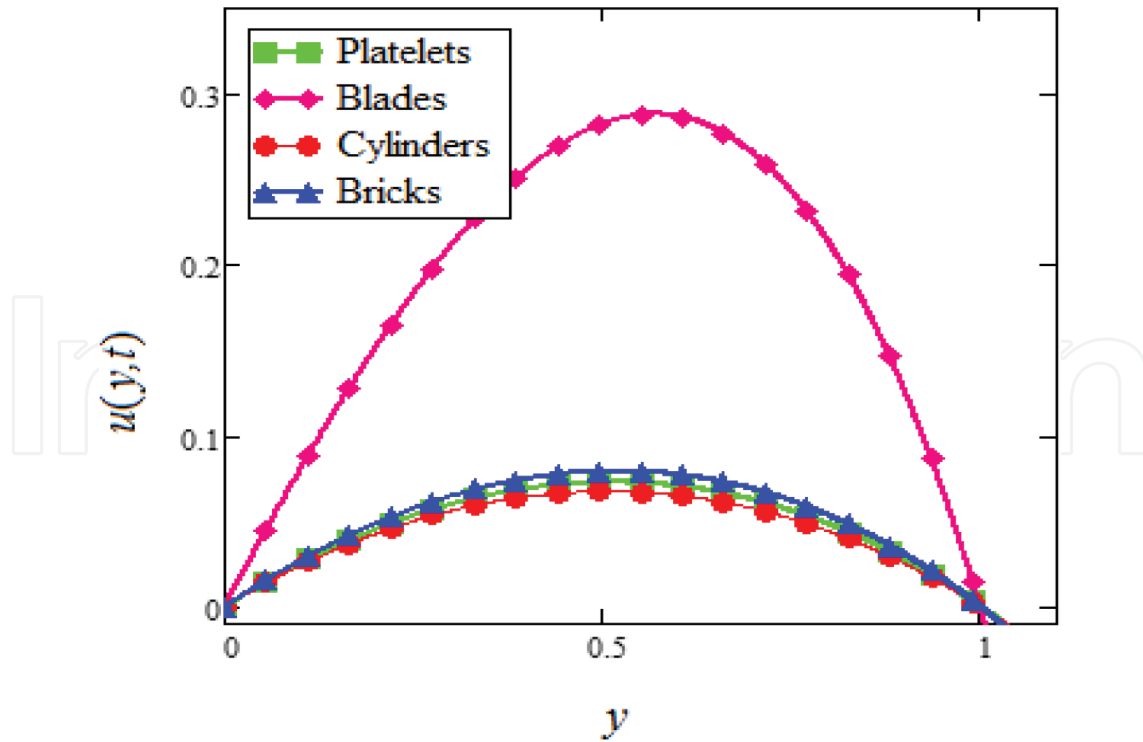
Figure 3. Velocity profiles for different shapes of Al_2O_3 nanoparticles in water-based nanofluids when $Gr = 0.1$, $N = 0.1$, $M = 1$, $\lambda = 1$, $K = 1$, $t = 5$, $\phi = 0.04$, $\omega = 0.2$.

nanoparticles in ethylene glycol-based nanofluids have the uppermost velocity chased by platelet, brick, and blade. Thus, in accordance with Hamilton and Crosser model, solution of elongated and thin shaped particles (high shape factor m) should have larger thermal conductivities, if the ratio of k_{nf}/k_f is higher than 100. It is also predicted by Colla et al. that the thermal conductivity and viscosity increase with the increase of particle absorption due to which motion of nanofluids decreases. For that reason, the cylindrical-shaped alumina Al_2O_3 nanoparticles have the higher thermal conductivity chased by platelet, brick, and blade. Timofeeva et al. depicted the conclusion that, when the sphericity of nanoparticles is less than 0.6, the negative concession of heat flow resistance at the solid-liquid interface increases much faster than the particle shape concession. Thus, the inclusive thermal conductivity of solution starts decreasing less than sphericity of 0.6. However, it is increasing in the case of Hamilton and Crosser model because of the only concession of particle shape parameter m. Nevertheless, flow in this work is one-directional and one-dimensional; therefore, the negative concession of heat flow resistance is ignored. Timofeeva et al. reported the model $k_{nf}/k_f = 1 + (c_k^{shape} + c_k^{surface})\, \phi$, for calculating the thermal conductivity of nanoparticles. In accordance with this model, c_k^{shape} and $c_k^{surface}$ coefficients reflecting concessions to the effective thermal conductivity because of particle shape (positive influence) and because of surface resistance (negative effect), respectively. Particle shape coefficient c_k^{shape} was also derived from the Hamilton and Crosser's equation (1962).

A comparability of alumina Al_2O_3 in $C_2H_6O_2$-based nanofluids with alumina Al_2O_3 in H_2O-based nanofluids is shown in **Figure 4**. It is viewed that the motion of H_2O-based nanofluids is larger than the motion of $C_2H_6O_2$-based nanofluids. The thermal conductivity and viscosity of $C_2H_6O_2$- and H_2O-based nanofluids are also perceived by the Hamilton and Crosser model for equal value of ϕ. This consequence shows that $C_2H_6O_2$-based nanofluids have larger thermal conductivity and viscosity than H_2O-based nanofluids.

The influence of different solid nanoparticles on the motion of different nanofluids is shown in **Figure 5**. From this figure, it is notable that cylindrical-shaped Al_2O_3 in $C_2H_6O_2$-based nanofluids has the uppermost motion chased by Fe_3O_4, TiO_2, Cu, and Ag in $C_2H_6O_2$-based nanofluids. This indicates that cylindrical-shaped silver Ag in $C_2H_6O_2$-based nanofluids has the higher viscosity and thermal conductivity assimilated to Cu, TiO_2, Fe_3O_4, and Al_2O_3 in $C_2H_6O_2$-based nanofluids. One can view from this consequence that cylindrical-shaped Ag in $C_2H_6O_2$-based nanofluids has better quality fluids assimilated to Fe_3O_4 cylindrical-shaped in $C_2H_6O_2$-based nanofluids. This consequence is supported by the Hamilton and Crosser model that the viscosity and thermal conductivity of nanofluids are also influenced by nanoparticles ϕ, i.e., the viscosity and thermal conductivity increase with the increase in ϕ. Therefore, motion decreases with the increase in ϕ. This figure further shows that the viscosity of Al_2O_3 in $C_2H_6O_2$-based nanofluids at ϕ is below 0.1, which increases nonlinearly with nanoparticles suspension. This consequence is found similar to the experimental consequence predicted by Colla et al.

Different ϕ of nonspherical cylindrical-shaped alumina Al_2O_3 nanoparticles on the motion of alumina Al_2O_3 in $C_2H_6O_2$-based nanofluids is exhibited in **Figure 6**. It is view from this figure that with the increase of ϕ the motion of nanofluids is decreased. Due to this reason, the
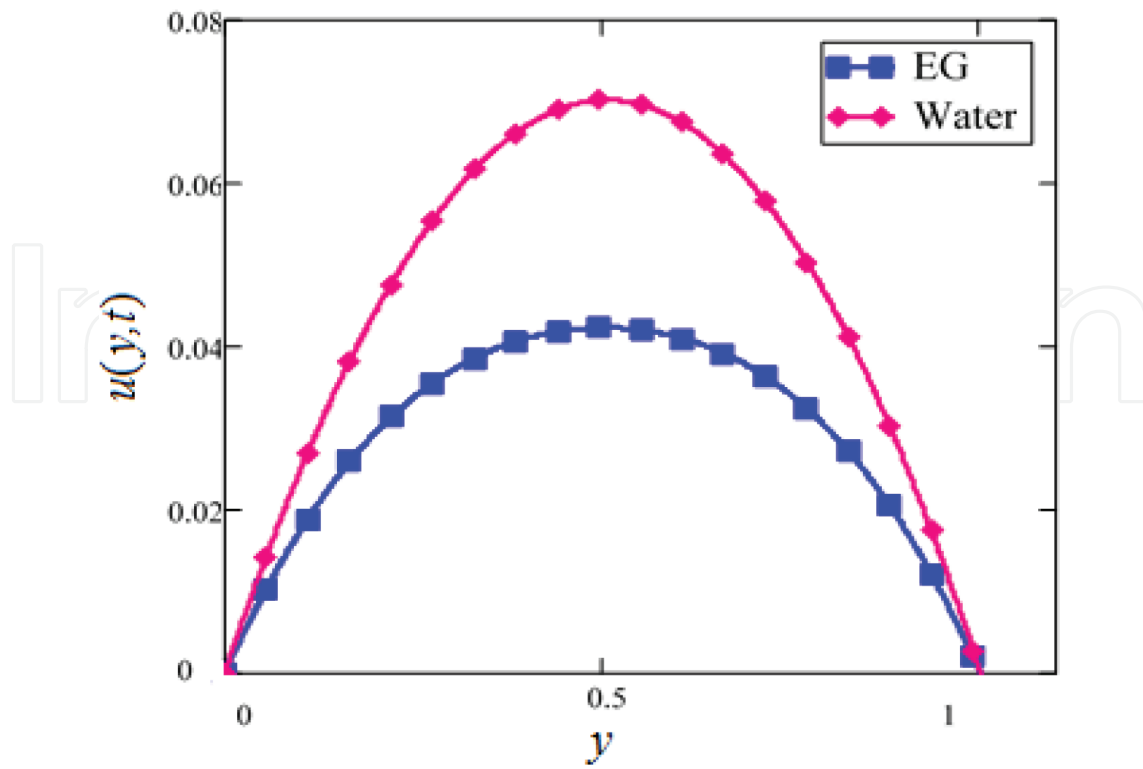
Figure 4. Comparison of velocity profiles of Al_2O_3 in EG and water-based nanofluids when $Gr = 0.1$, $N = 0.1$, $M = 1$, $\lambda = 1$, $K = 1$, $t = 5$, $\phi = 0.04$, $\omega = 0.2$.
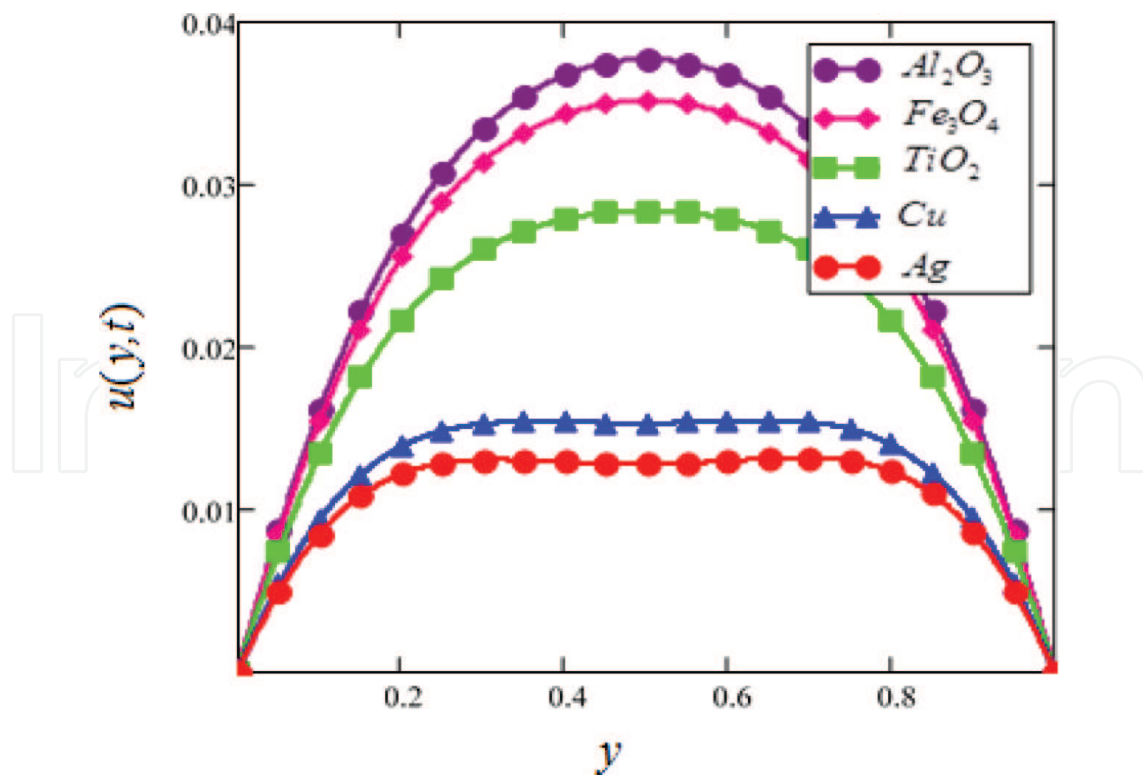

Figure 5. Velocity profiles of different nanoparticles in EG-based nanofluids when $Gr = 0.1$, $N = 0.1$, $M = 1$, $\lambda = 1$, $K = 1$, $t = 5$, $\phi = 0.04$, $\omega = 0.2$.
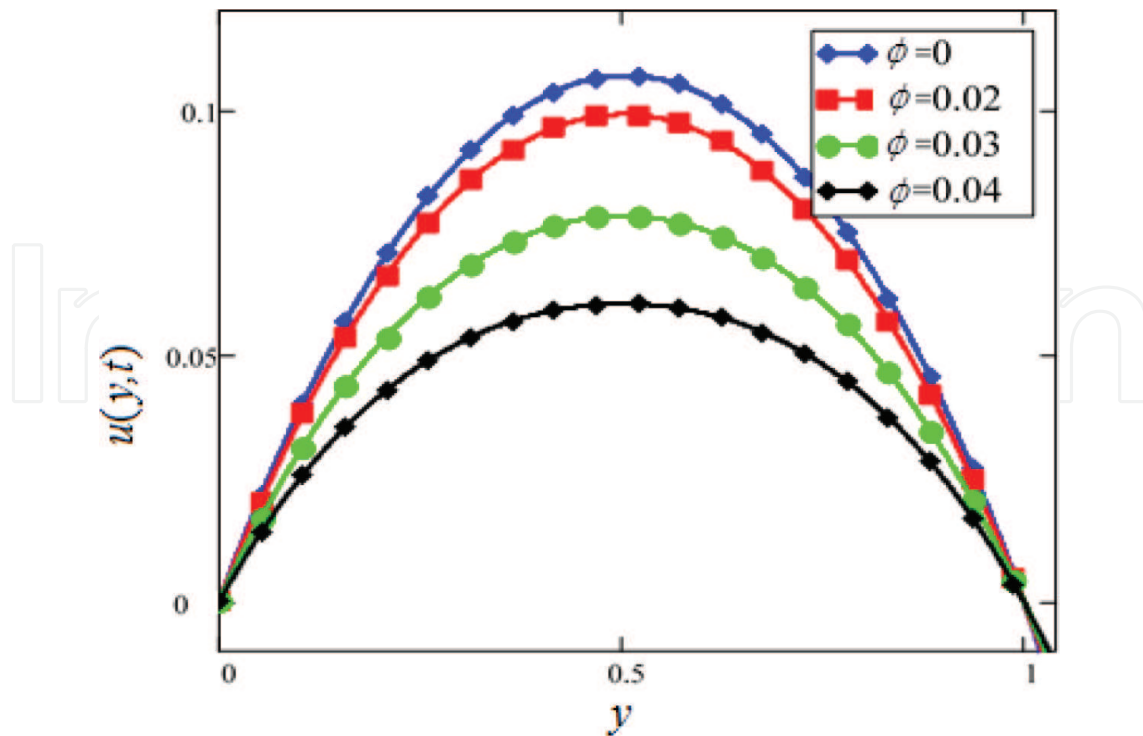
Figure 6. Velocity profiles for different values of ϕ of Al_2O_3 in EG-based nanofluids when $Gr = 0.1$, $N = 0.1$, $M = 1$, $\lambda = 1$, $K = 1$, $t = 5$, $\omega = 0.2$.

nanofluid becomes more viscous with the increase of ϕ, which governs to decrease the motion of nanofluids. The thermal conductivity of nanofluids also increases with the increase of ϕ. The experimental research by Colla et al. also supports these results.

Consequences for various values of radiation parameter N of Al_2O_3 in H_2O-based nanofluids are displayed in **Figure 7**. It is observed that motion increases with the increase of N. This consequence agrees well with the consequence reported by Makinde and Mhone. Physically, this means that with the increase of N, the amount of heat energy transfers to the fluids also increases.

The graphical outcomes of the motion of nanofluids for several values of magnetic parameter M of alumina Al_2O_3 in H_2O-based nanofluids are exhibited in **Figure 8**. Increasing magnetic parameter, M, results in the decrease of the motion of the alumina nanofluids. Increasing perpendicular magnetic field on the electrically conducting fluid imparts to a resistive force called Lorentz force, which is identical to drag force, and upon increasing the value of magnetic parameter, M, the drag force rises which has the tendency to reduce the motion of the nanofluid. The resistive force is maximum near the plates of the channel and minimum in the middle of the plates. Therefore, motion on the alumina nanofluids is maximum in the middle of the plates and minimum at the plates. The motion of alumina nanofluids for various numerical values of Grashof number, Gr of Al_2O_3 in H_2O-based nanofluids is shown in **Figure 9**. It is concluded that an increase in Grashof number, Gr, governs to an increase in the motion of alumina nanofluids. An increase in Grashof number, Gr, rises temperature of alumina in ethylene glycol nanofluids, which govern to an increase in the upward buoyancy force. Therefore, motion in alumina nanofluids increases with Gr, because of the increment of buoyancy force. **Figure 10** shows
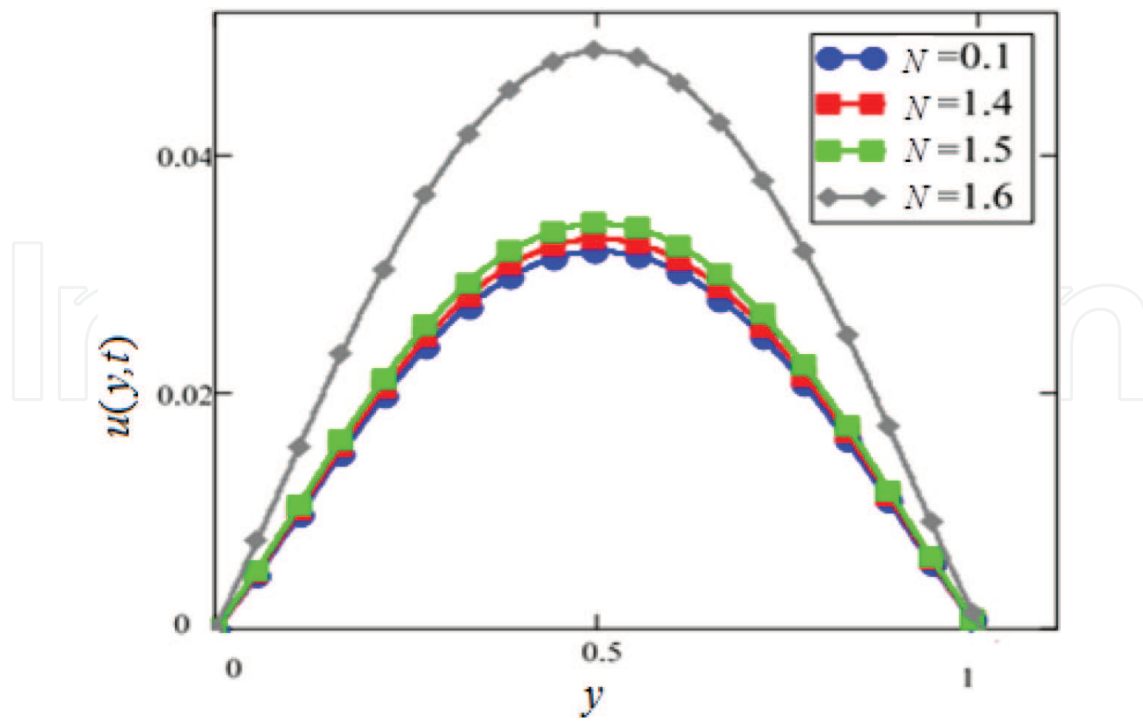
Figure 7. Velocity profiles for different values of N of Al_2O_3 in EG-based nanofluids when $Gr = 0.1$, $M = 1$, $\lambda = 1$, $K = 1$, $t = 5$, $\phi = 0.04$, $\omega = 0.2$.
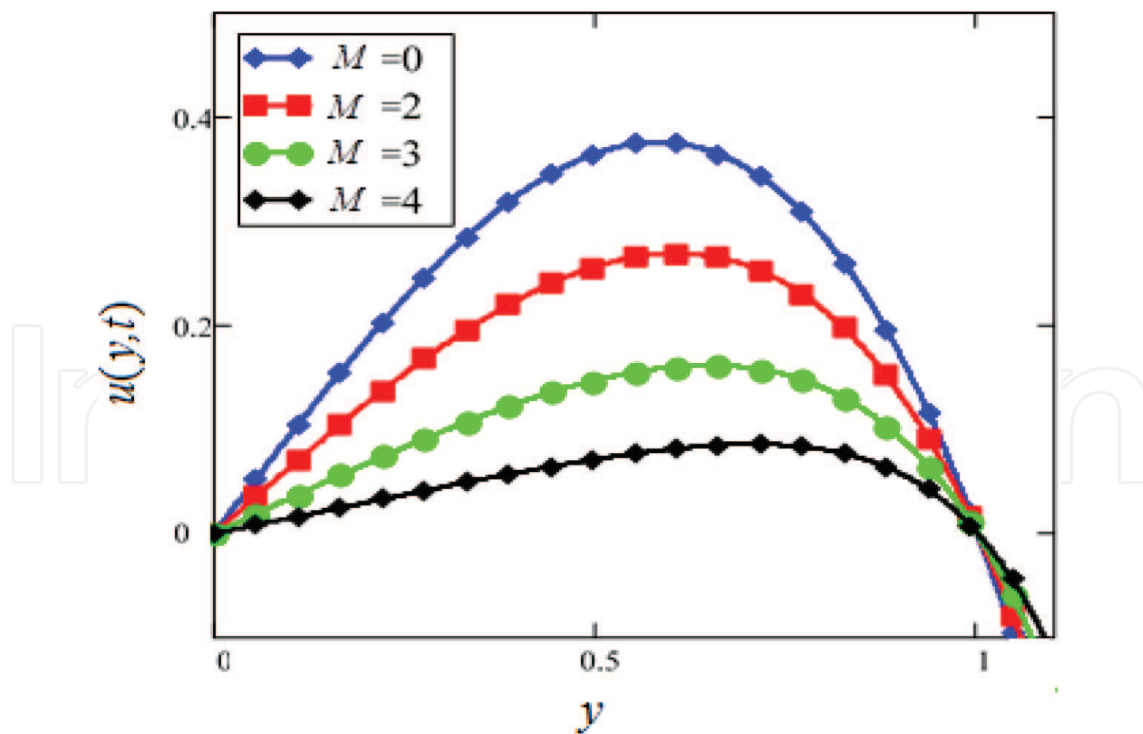

Figure 8. Velocity profiles for different values of M of Al_2O_3 in EG-based nanofluids when $Gr = 0.1$, $N = 0.1$, $\lambda = 1$, $K = 1$, $t = 5$, $\phi = 0.04$, $\omega = 0.2$.
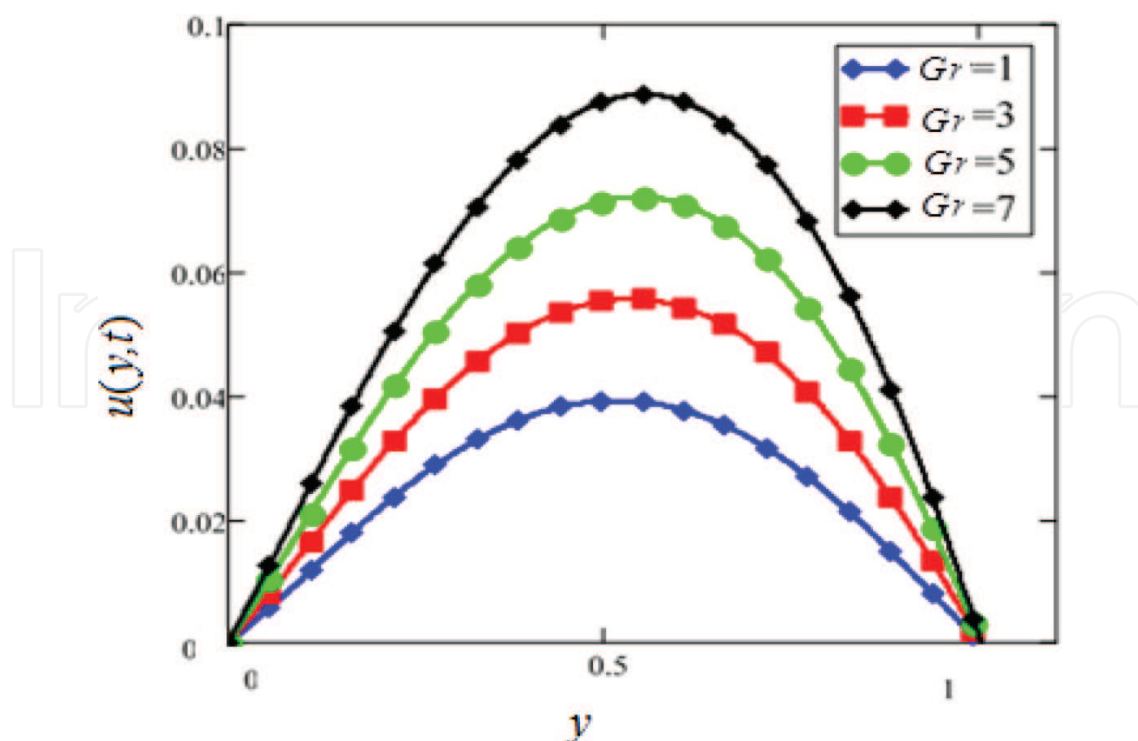
Figure 9. Velocity profiles for different values of Gr of Al_2O_3 in EG-based nanofluids when $N = 0.1$, $M = 1$, $\lambda = 1$, $K = 1$, $t = 10$, $\phi = 0.04$, $\omega = 0.2$.

permeability parameter K. It is view that motion of Al_2O_3 in $C_2H_6O_2$-based nanofluids increases with increasing values of permeability parameter K of Al_2O_3 in $C_2H_6O_2$-based nanofluids because of the small friction force. Similarly, increasing K reduces the nanofluids friction within the plate walls and motion of alumina nanofluids enhances. In the second case, **Figures 11–18** show the flow condition when the left wall is oscillating in its own plane and the right wall is stationary. Under the last conditions, when both plates of the channel are oscillating in their planes (**Figures 19–26**). From all these graphs, we found that they are qualitatively identical but different quantitatively to **Figures 2–10**. It can also viewed from **Figures 11**, **13**, and **14** that the motion of Al_2O_3 in $C_2H_6O_2$-based nanofluids at the right wall ($y = 1$) is not equal to zero. It is because of the reason of oscillating right plate of the channel. It should also be investigated from **Figures 20**, **24**, and **26** that only the magnitude of motion of nanofluids is considered; therefore, the negative sign in motion is ignored in these figures and only shows that the motion of Al_2O_3 in $C_2H_6O_2$-based nanofluids is reduced.

The influence of dissimilar particle shapes on the temperature of Al_2O_3 in H_2O and $C_2H_6O_2$-based nanofluids is presented in **Figures 27** and **28**. The temperature of both types of nanofluids is different for dissimilar shapes because of the various viscosity and thermal conductivity of these nanoparticles. It should be concluded that the influence of thermal conductivity increases with the increase of temperature. However, the viscosity decreases with the increase of temperature. It is view that an elongated shape of nanoparticles inside H_2O-based nanofluids like cylinder and platelet has small temperature due to the larger viscosity and thermal conductivity while the blade shape of nanoparticles has the uppermost temperature because of least viscosity and thermal conductivity. The brick shape nanoparticles suspended fluids are lowest in the temperature range; however, it has low viscosity. This is
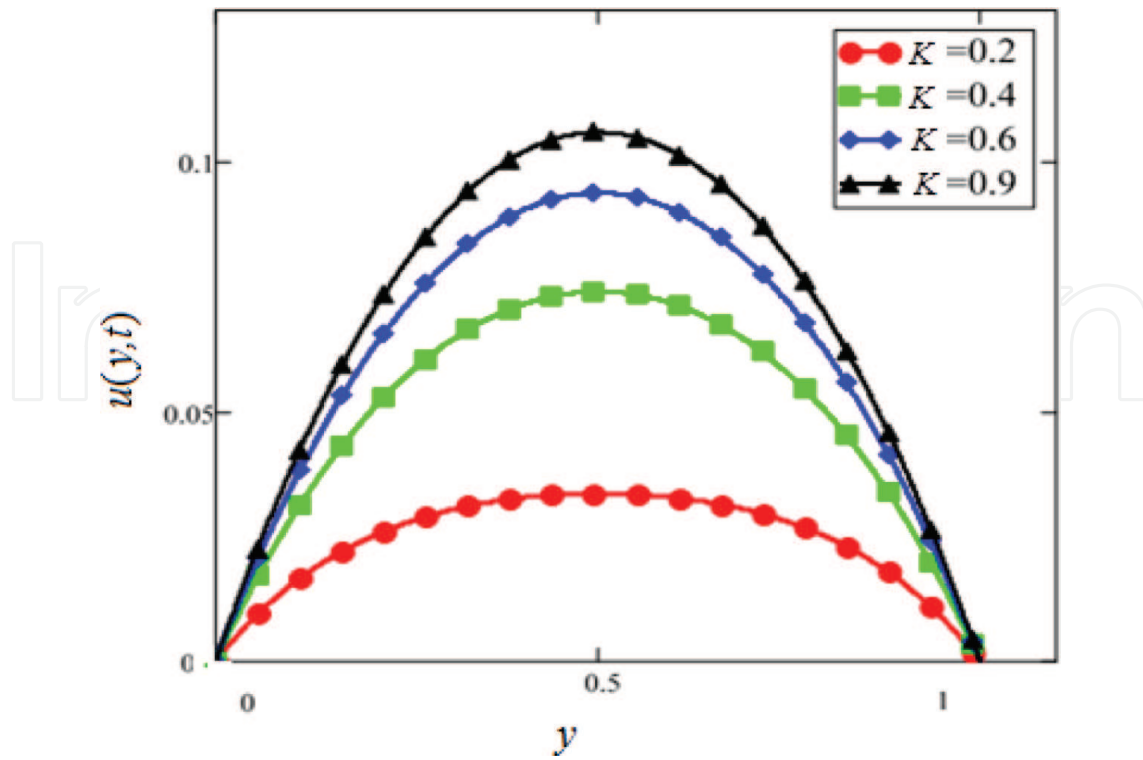
Figure 10. Velocity profiles of different valeus of K of Al_2O_3 in EG-based nanofluids when $Gr = 0.1$, $N = 0.1$, $M = 1$, $\lambda = 1$, $t = 5$, $\phi = 0.04$, $\omega = 0.2$.
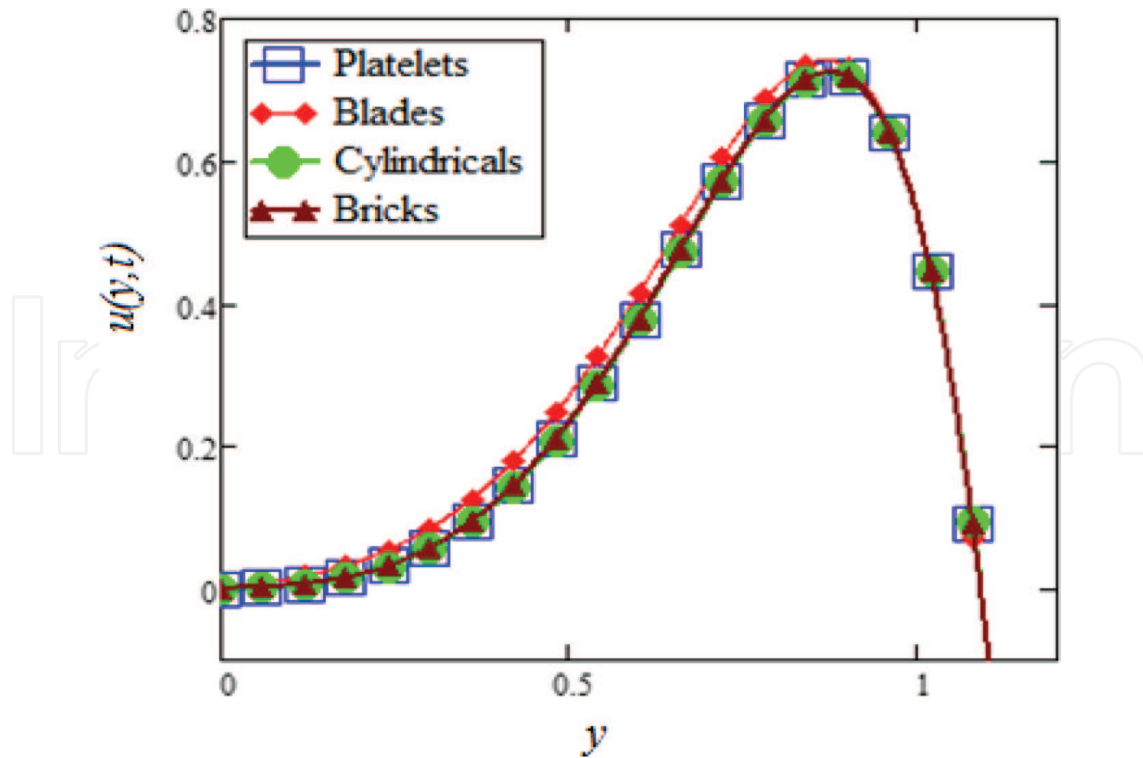

Figure 11. Velocity profiles for different shapes of Al_2O_3 nanoparticles in EG-based nanofluids when $Gr = 0.1$, $N = 0.1$, $M = 1$, $\lambda = 1$, $K = 1$, $t = 5$, $\phi = 0.04$, $\omega = 0.2$.
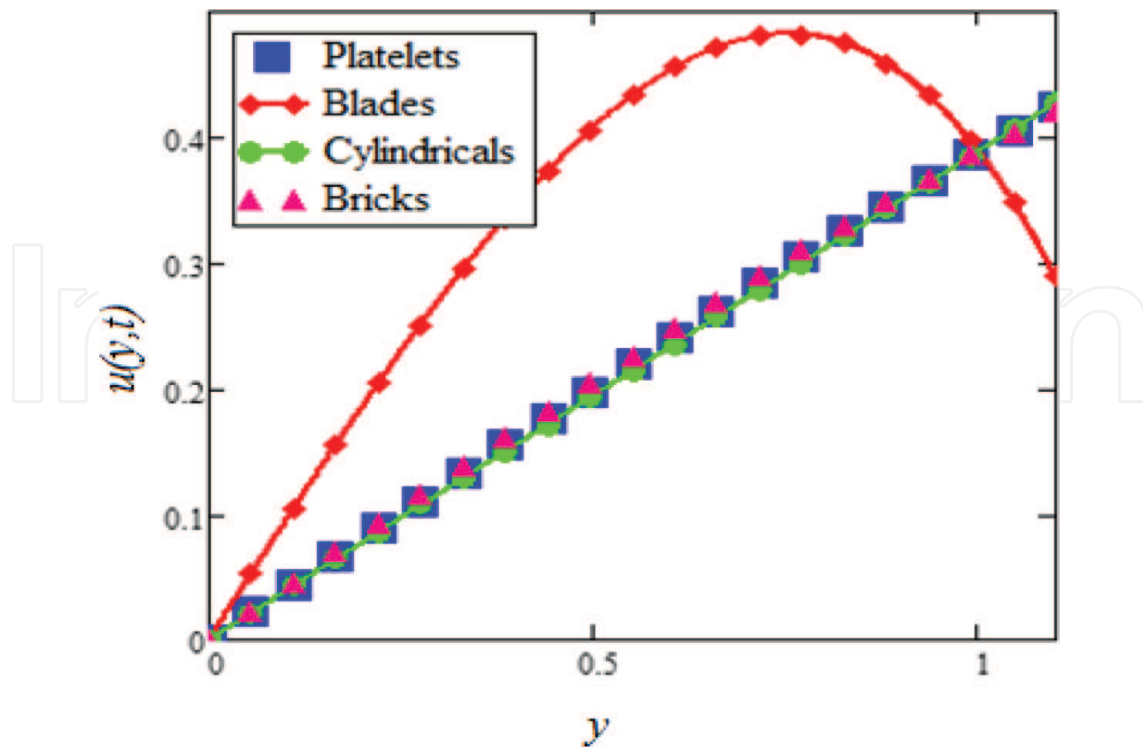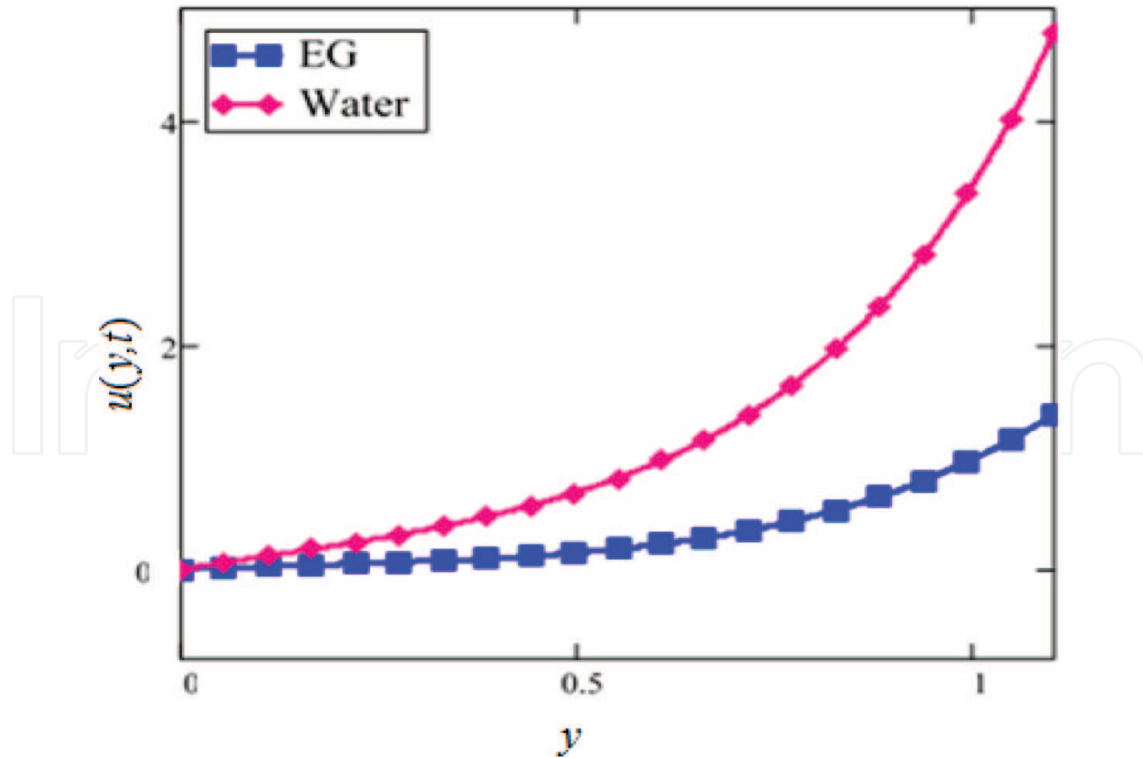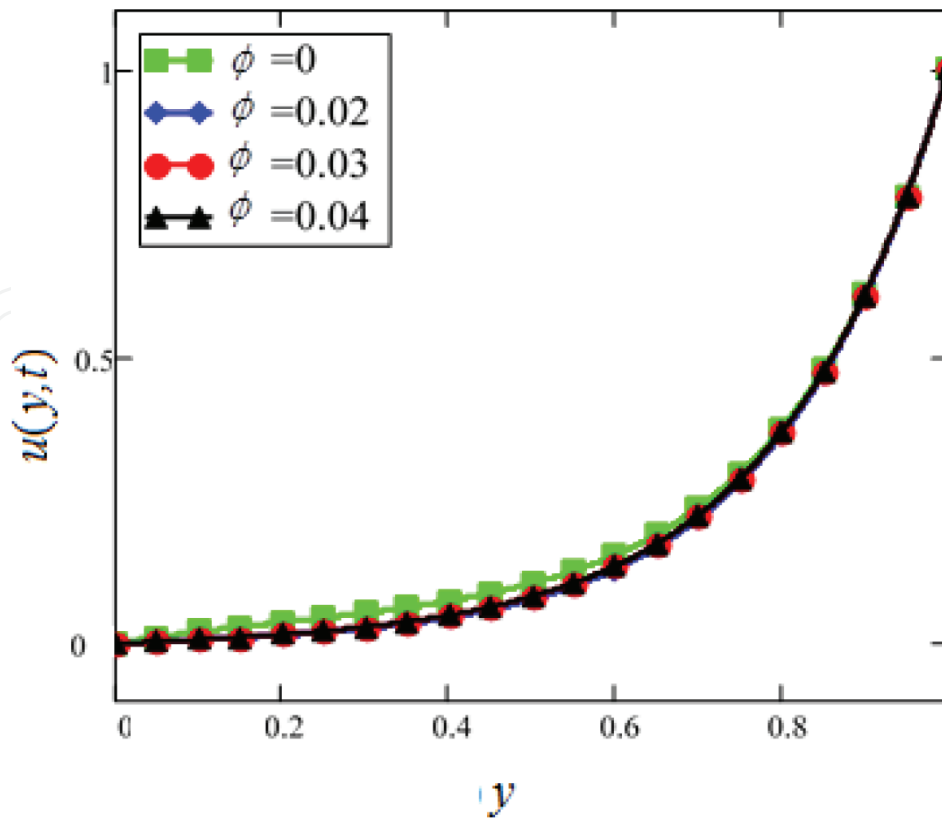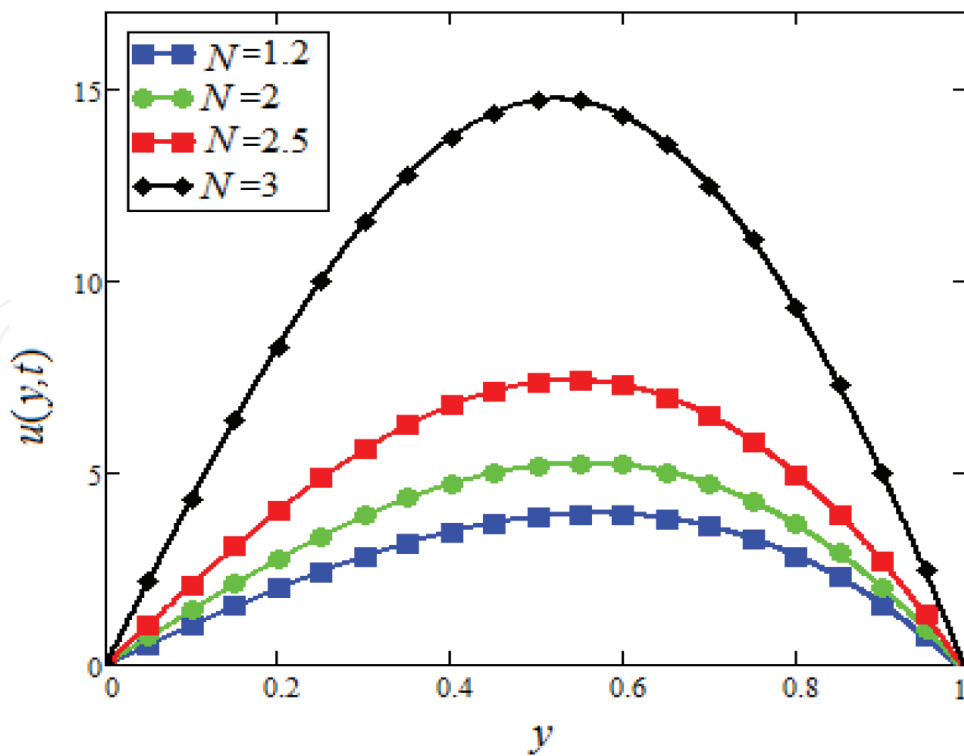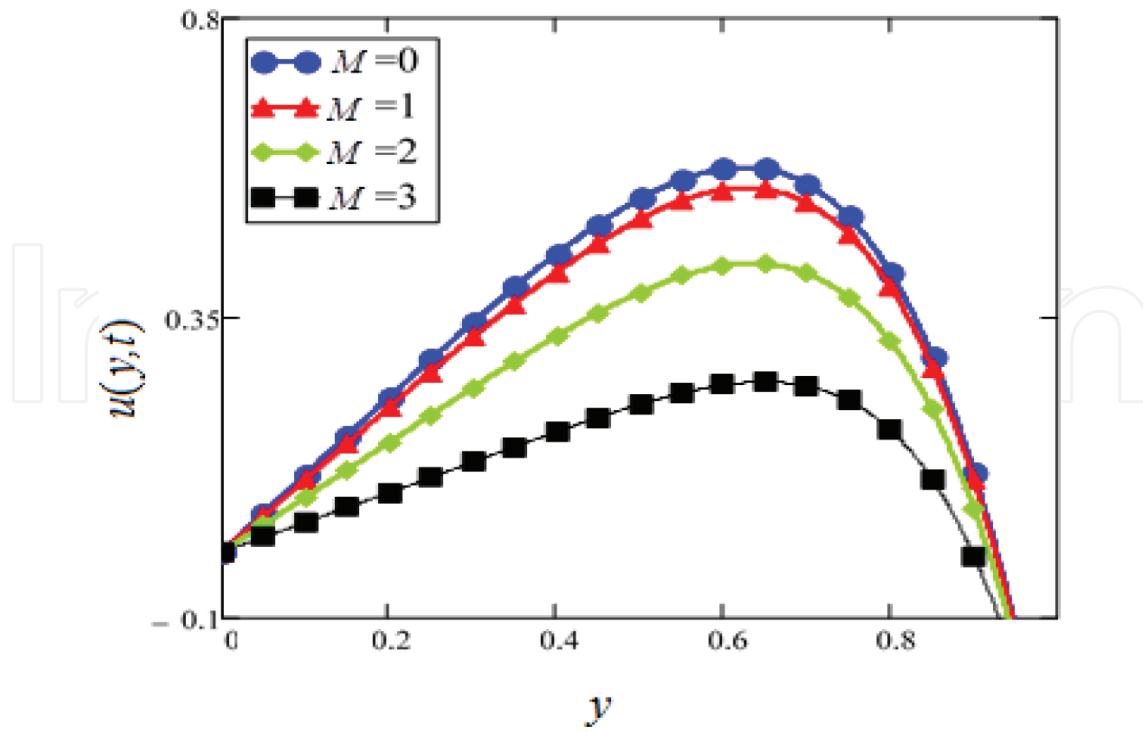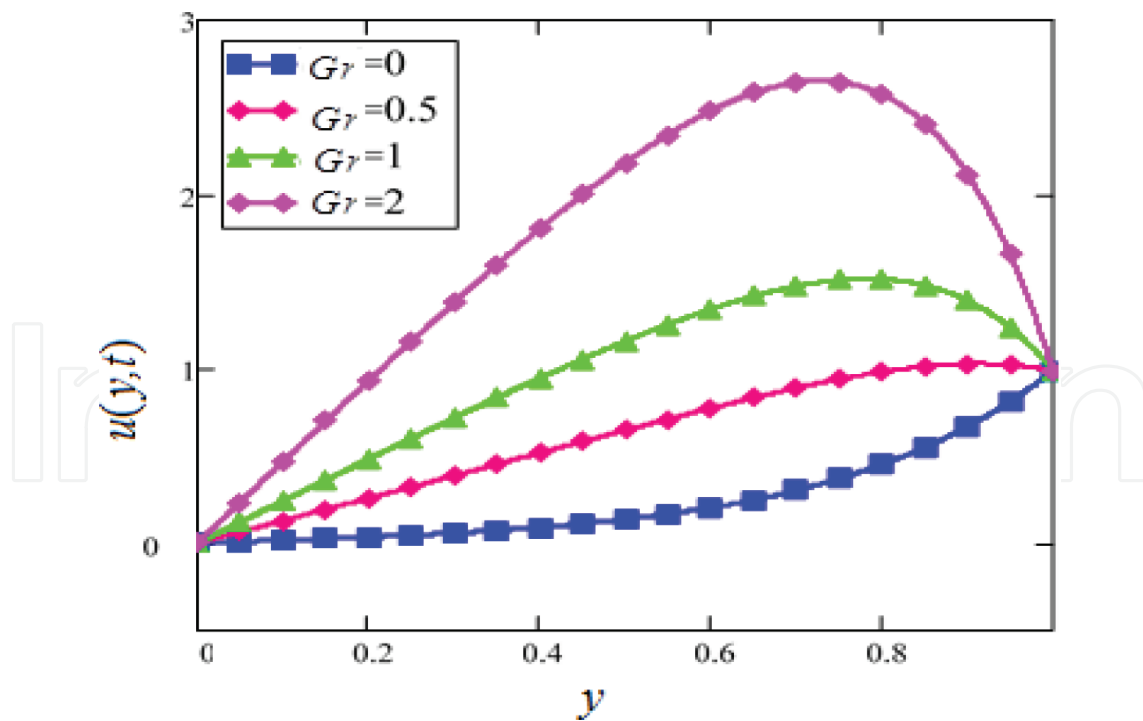
Figure 12. Velocity profiles for different shapes of Al_2O_3 nanoparticles in water-based nanofluids when $Gr = 0.1$, $N = 0.1$, $M = 1$, $\lambda = 1$, $K = 1$, $t = 5$, $\phi = 0.04$, $\omega = 0.2$.

Figure 13. Comparison of velocity profiles of Al_2O_3 in EG- and water-based nanofluids when $Gr = 0.1$, $N = 0.1$, $M = 1$, $\lambda = 1$, $K = 1$, $t = 5$, $\phi = 0.04$, $\omega = 0.2$.

Figure 14. Velocity profiles for different values of ϕ of Al_2O_3 in EG-based nanofluids when $Gr = 0.1,\ \ N = 0.1,\ M = 1,$ $\lambda = 0.01,\ \ K = 0.3,\ \ t = 10,\ \ \omega = 0.2.$

Figure 15. Velocity profiles for different values of N of Al_2O_3 in EG-based nanofluids when $Gr = 1,\ M = 1,\ \ \lambda = 0.01,$ $K = 0.2,\ \ t = 10,\ \ \phi = 0.04,\ \ \omega = 0.2.$

Figure 16. Velocity profiles for different values of M of Al_2O_3 in EG-based nanofluids when $Gr = 1$, $N = 0.1$, $\lambda = 0.001$, $K = 1$, $t = 10$, $\phi = 0.04$, $\omega = 0.2$.

Figure 17. Velocity profiles for different values of Gr of Al_2O_3 in EG-based nanofluids when $N = 0.1$, $M = 1$, $\lambda = 0.01$, $K = 0.2$, $t = 10$, $\phi = 0.04$, $\omega = 0.2$.

because of the shear thinning behavior with temperature of nanofluids. Moreover, cylindrical-shaped nanofluids also show shear thinning behavior. However, the effect is less dominant. All

the other dissimilar shapes like platelet and blade show Newtonian behavior and independence of viscosity on shear rate. This shear thinning behavior is also analyzed experimentally by Timofeeva et al.
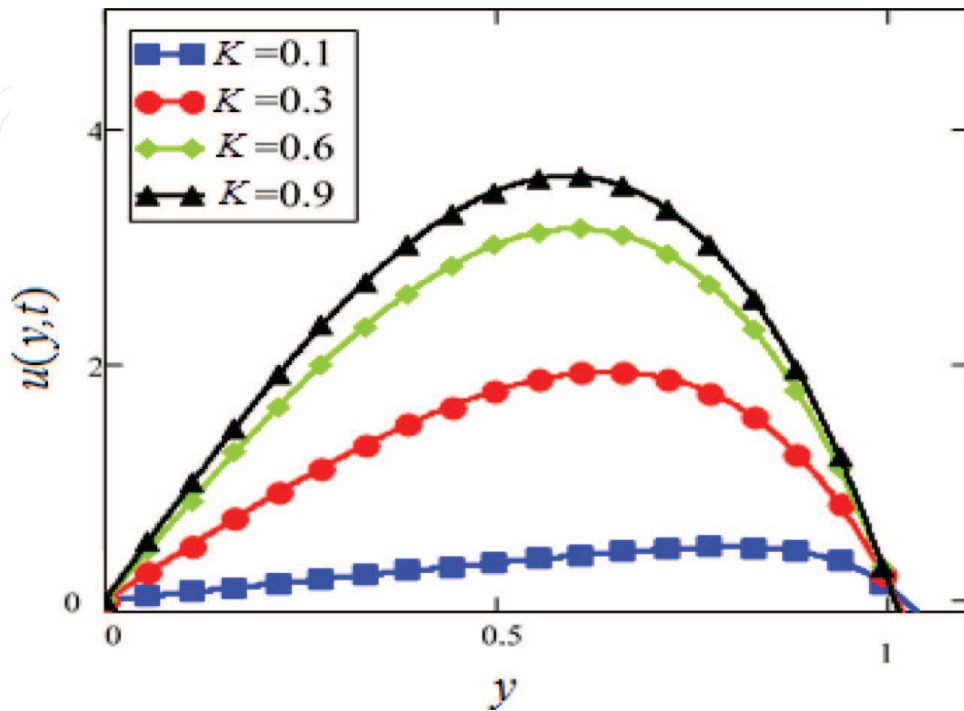

Figure 18. Velocity profiles for different values of K of Al_2O_3 in EG-based nanofluids when $Gr = 0.1$, $N = 0.1$, $M = 1$, $\lambda = 0.01$, $t = 10$, $\phi = 0.04$, $\omega = 0.2$.
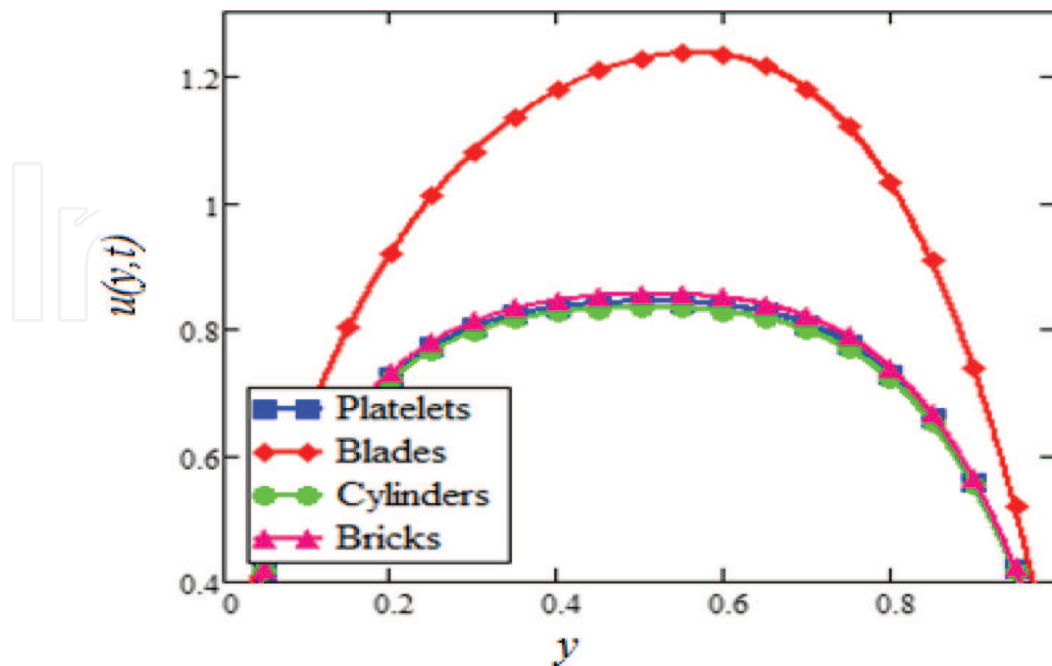

Figure 19. Velocity profiles for different shapes of Al_2O_3 nanoparticles in EG-based nanofluids when $Gr = 1$, $N = 0.1$, $M = 1$, $\lambda = 0.01$, $K = 1$, $t = 10$, $\phi = 0.04$, $\omega = 0.2$.
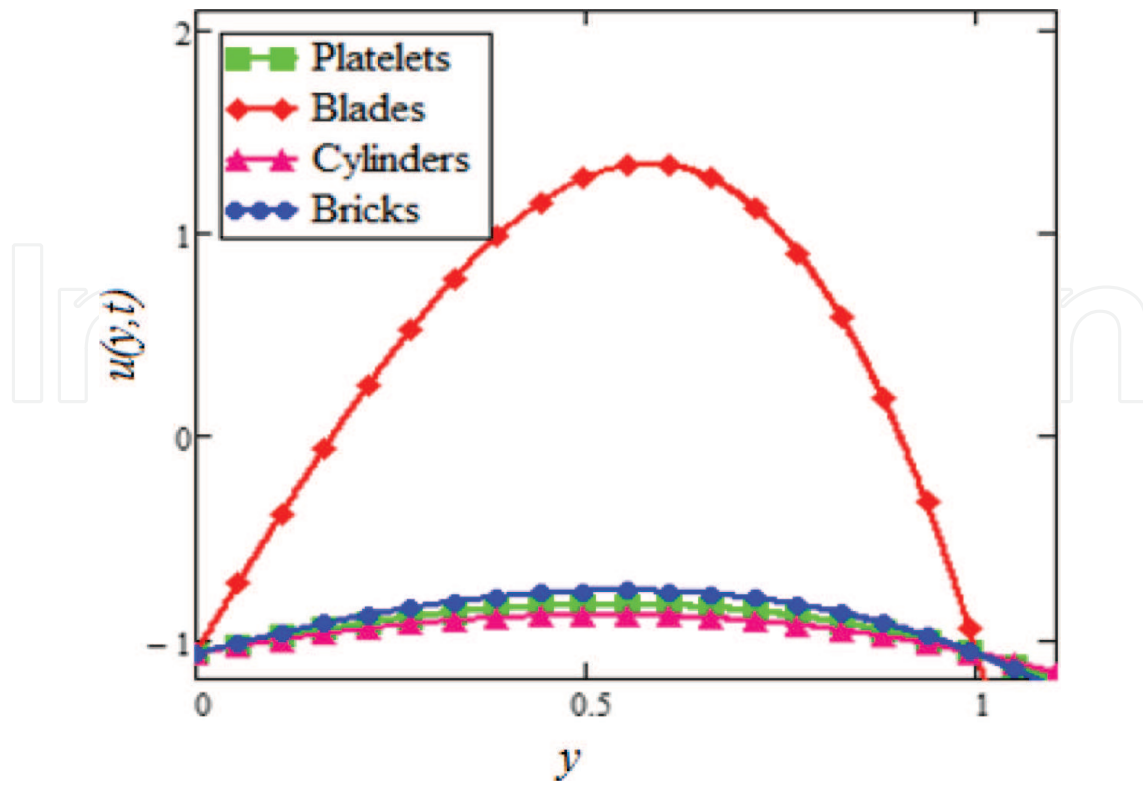
Figure 20. Velocity profiles for different shapes of Al_2O_3 nanoparticles in water-based nanofluids when $Gr = 1$, $N = 0.1$, $M = 1$, $\lambda = 0.01$, $K = 1$, $t = 10$, $\phi = 0.04$, $\omega = 0.2$.
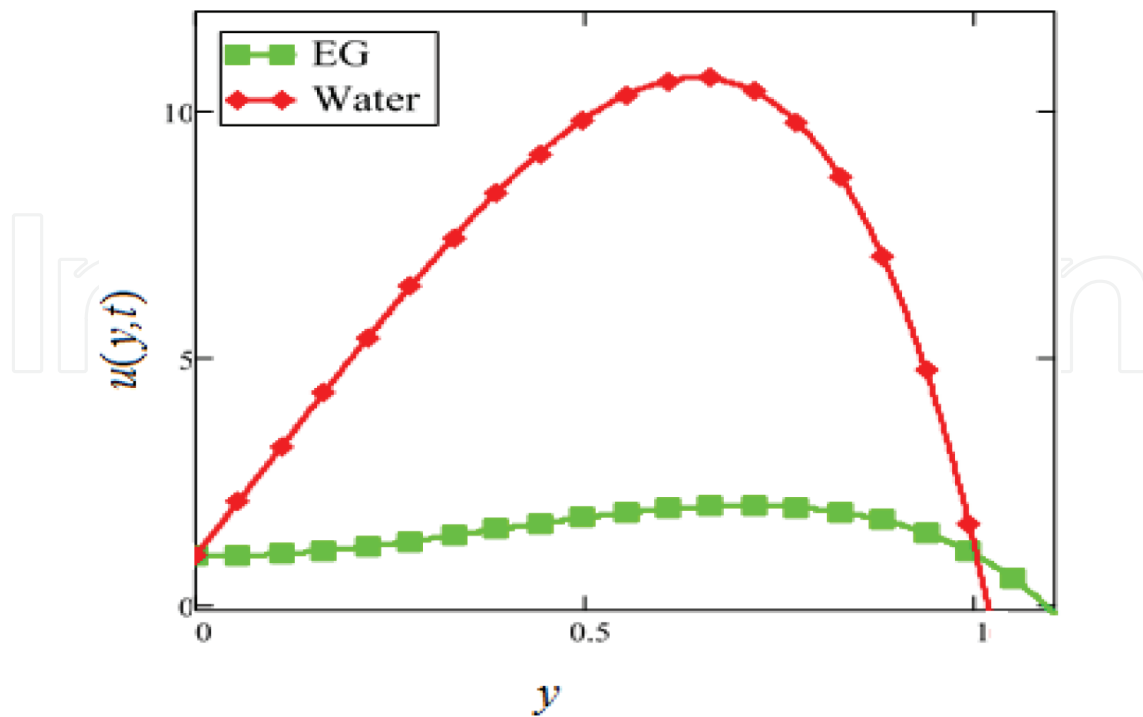

Figure 21. Comparison of velocity profiles of Al_2O_3 in EG- and water-based nanofluids when $Gr = 1$, $N = 0.1$, $M = 1$, $\lambda = 0.01$, $K = 1$, $t = 10$, $\phi = 0.04$, $\omega = 0.2$.
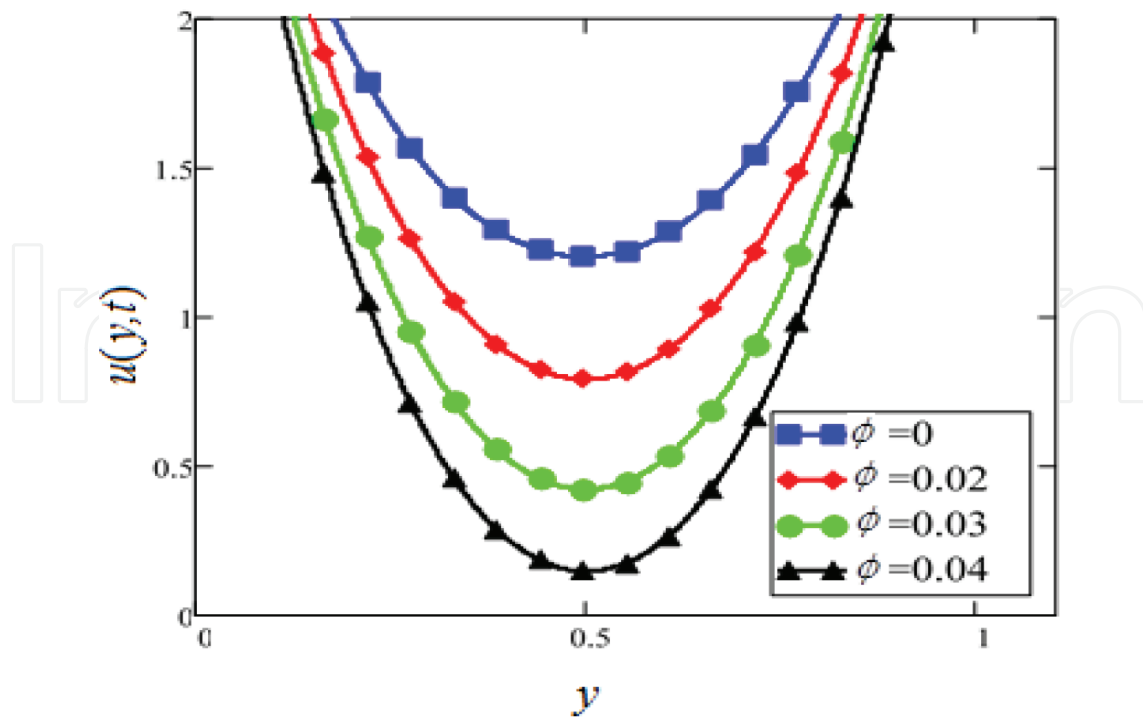
Figure 22. Velocity profiles for different values of ϕ of Al$_2$O$_3$ in EG-based nanofluids when $Gr = 1$, $N = 0.1$, $M = 1$, $\lambda = 0.01$, $K = 1$, $t = 10$, $\omega = 0.2$.

Figure 23. Velocity profiles for different values of N of Al$_2$O$_3$ in EG-based nanofluids when $Gr = 1$, $M = 1$, $\lambda = 0.01$, $K = 1$, $t = 10$, $\phi = 0.04$, $\omega = 0.2$.
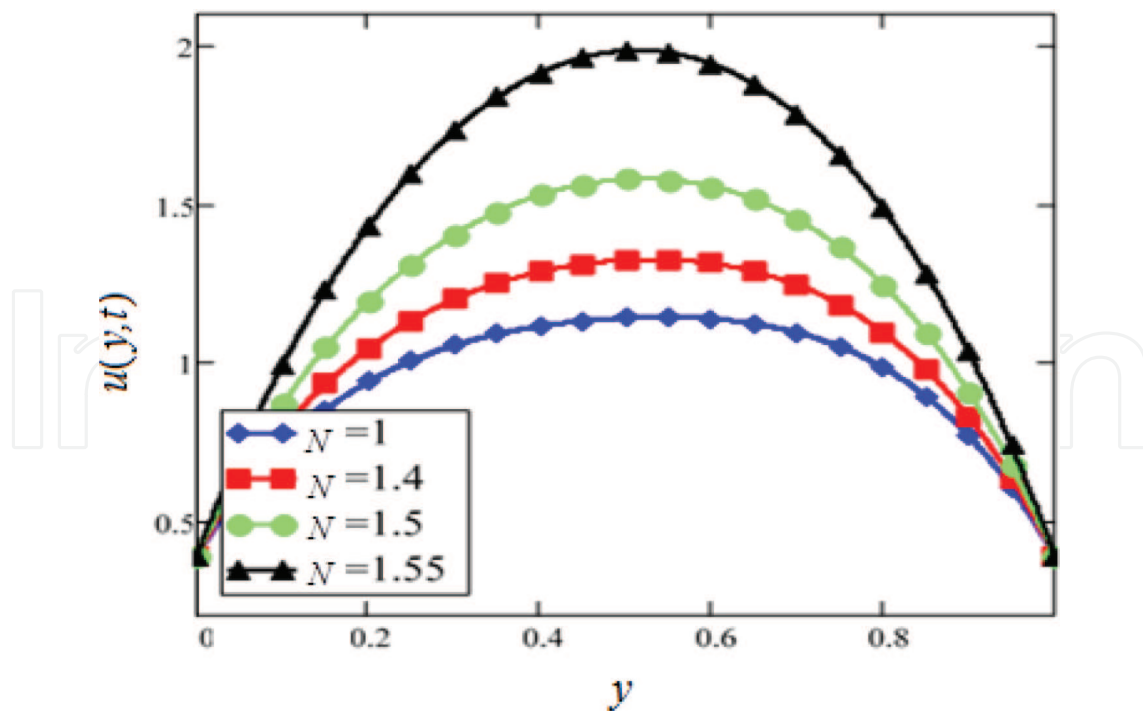
Figure 24. Velocity profiles for different values of M of Al_2O_3 in EG-based nanofluids when $Gr = 1$, $M = 1$, $\lambda = 0.01$, $K = 1$, $t = 10$, $\phi = 0.04$, $\lambda = 0.01$, $\omega = 0.2$.

Figure 25. Velocity profiles for different values of Gr of Al_2O_3 in EG-based nanofluids when $Gr = 1$, $M = 1$, $\lambda = 0.01$, $K = 1$, $t = 10$, $\phi = 0.04$, $\omega = 0.2$.

Figure 26. Velocity profiles for different values of K of Al_2O_3 in EG-based nanofluids when $Gr = 1$, $M = 1$, $\lambda = 0.01$, $K = 1$, $t = 10$, $\phi = 0.04$, $\omega = 0.2$.
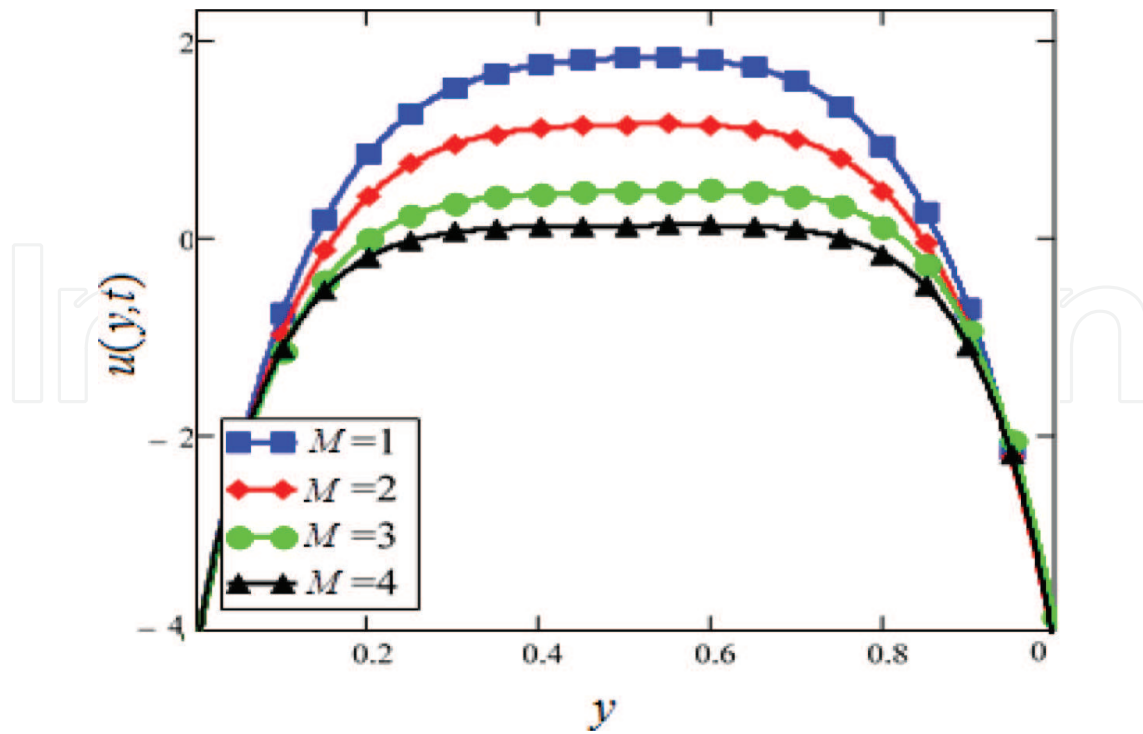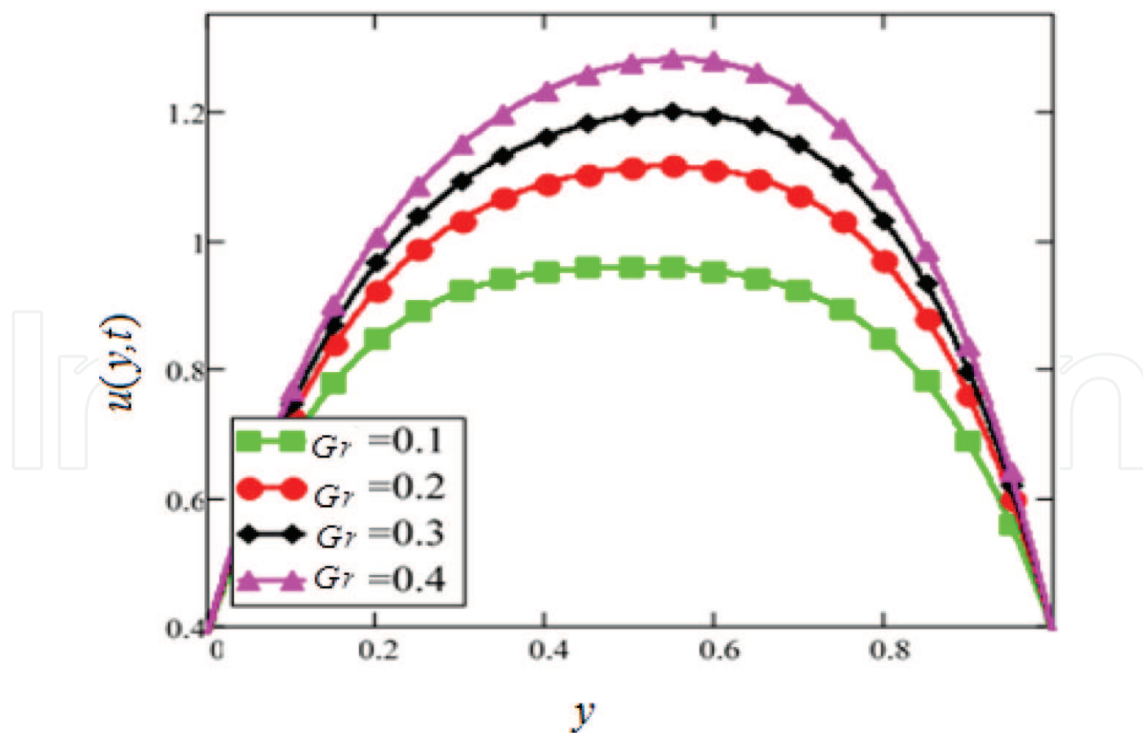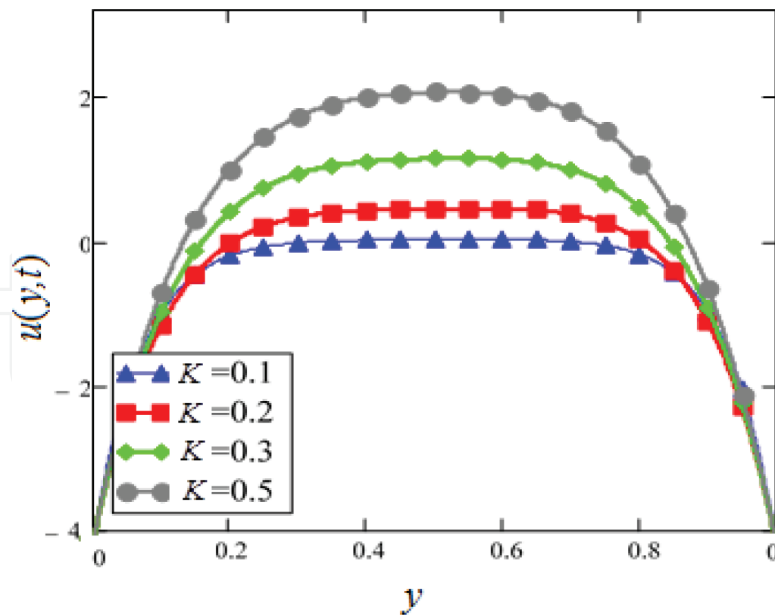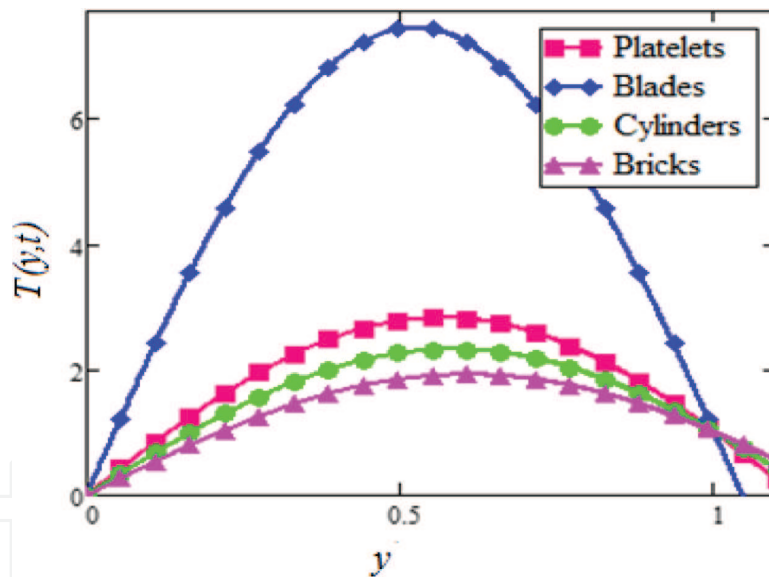

Figure 27. Temperature profiles for different shapes of Al_2O_3 nanoparticles in EG-based nanofluids when $N = 1.5$, $t = 1$.

A comparatively study of Al_2O_3 in H_2O- and $C_2H_6O_2$-based nanofluids is displayed in **Figure 29**. It is analyzed that both nanofluids are temperature dependent and the variation is found at the same rate for both types of nanofluids. This means that the influence of temperature of nanofluids on the thermal conductivity and viscosity of two types of base nanofluids may cause at the same rate. **Figure 30** exhibits the influence of ϕ on the temperature of Al_2O_3 in $C_2H_6O_2$-based nanofluids. It is evaluated that with the increase of ϕ temperature of the nanofluid increases because of the shear thinning nature. The viscosity of cylindrical-shaped nanoparticles inside water and $C_2H_6O_2$-based nanofluids shows shear thinning nature at the highest suspension. This was also experimentally investigated by Timofeeva et al.

The graphical consequences of temperature of nanofluids for several values of N are displayed in **Figure 31**. It is indicated that the temperature of the cylindrical-shaped alumina Al_2O_3 nanoparticles in $C_2H_6O_2$-based nanofluids shows larger oscillation with the increase of N. It is evaluated in the solution of the problem that temperature of the alumina nanofluids is oscillating and the influence of oscillation is increase with the increase of N. The increasing N means cooler or dense nanofluids or reduce the influence of energy transport to the nanofluids. The cylindrical-shape nanofluids have temperature dependent viscosity because of the shear thinning nature.

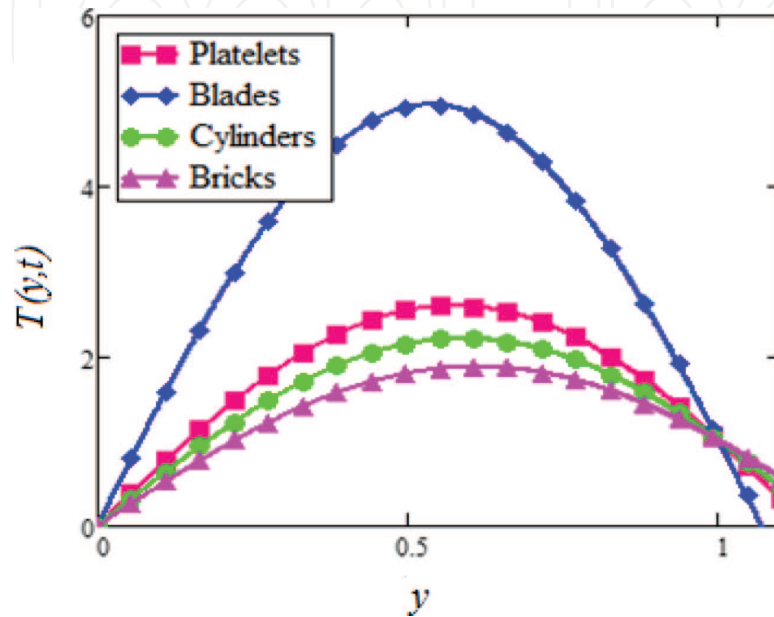**Figure 28.** Temperature profiles for different shapes of Al_2O_3 nanoparticles in water-based nanofluids when $N = 1.5$, $t = 1$.
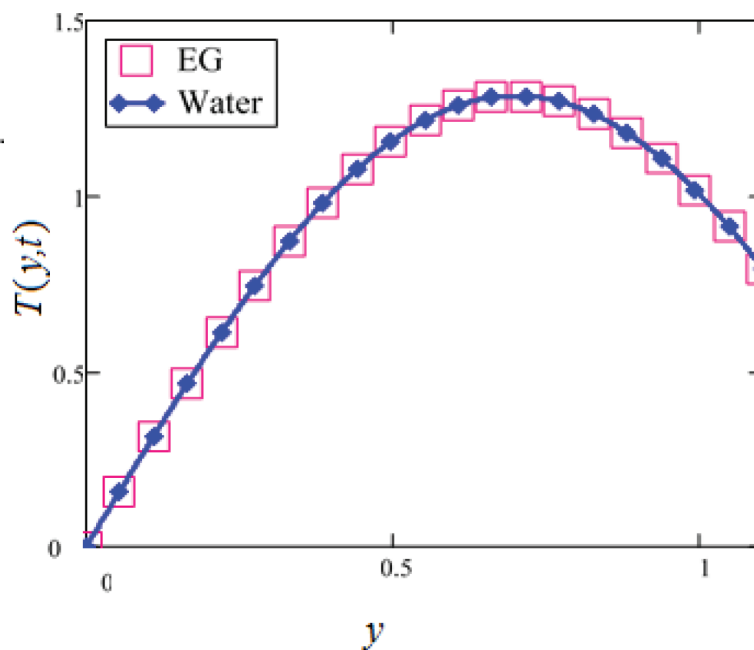

Figure 29. Comparison of temperature profiles of Al_2O_3 in EG- and water-based nanofluids when $N = 1.5$, $t = 1$.
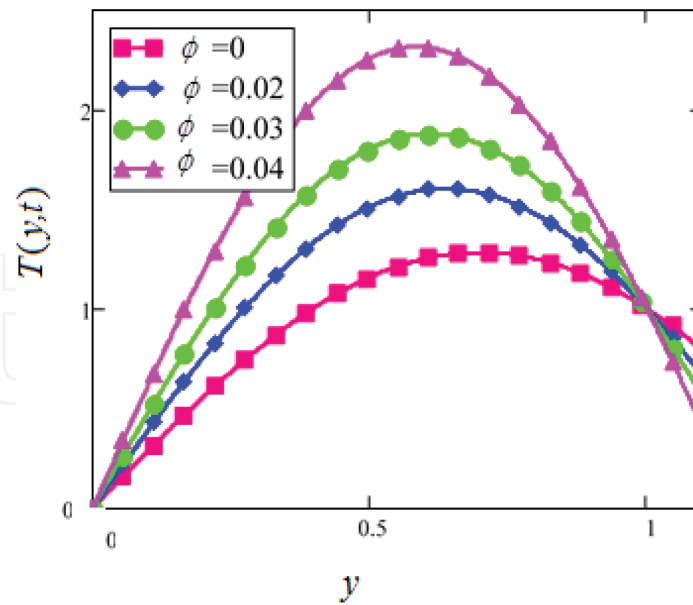
Figure 30. Temperature profiles for different values of ϕ of Al_2O_3 in EG-based nanofluids when $N = 1.5$, $t = 1$.
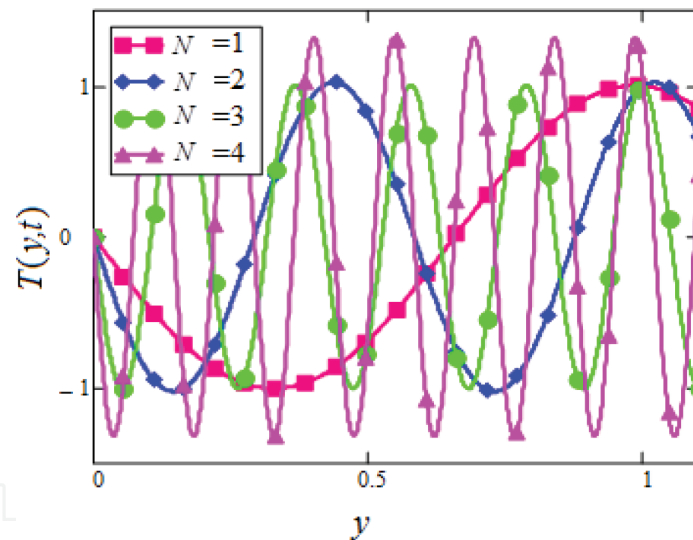
Figure 31. Temperature profiles for different values of N of Al_2O_3 in EG-based nanofluids when $t = 1$.

4. Conclusions

In this chapter, the influence of radiative heat transfer on mixed convection MHD flow of different shapes of Al_2O_3 in $C_2H_6O_2$, and H_2O base nanofluids in a channel filled with a saturated porous medium is analyzed. The two plates of the channel at finite distance with nonuniform wall temperature are chosen in a vertical direction under the influence of a perpendicular magnetic field. The governing PDEs are solved by the perturbation method for three different flow cases, and analytic solutions are evaluated. The influence of the dissimilar shapes of nanoparticles, namely, platelet, blade, cylinder, and brick of the same volume, on the motion

of nanofluids and temperature of nanofluids is examined with different consequences. An elongated shape of nanoparticles inside base fluids like cylinder and platelet results in greater viscosity at the equal volume fraction due to structural limitation of rotational and transitional Brownian motion. The shear thinning nature of cylinder and blade shape of nanoparticles inside H_2O and $C_2H_6O_2$ is also investigated in this research. Viscosities and thermal conductivities of nanofluids are viewed depending on nanoparticle shapes, suspension of volume fraction, and base fluid of solid nanoparticles. The concluded results are as follow:

1. The motion of nanofluid decreases with the increase of volume fraction of nanoparticles because of the increment in viscosity and thermal conductivity.

2. The motion of $C_2H_6O_2$ base nanofluid is found smaller than H_2O base nanofluid because the viscosity of base fluid influences the Brownian movement of the nanoparticles.

3. Elongated nanoparticles inside water and $C_2H_6O_2$ like cylinder and platelet shapes have smaller motion as assimilated to blade and brick shapes of nanoparticles because of greater viscosity.

4. The motion of the nanofluid decreases with the enhancement of magnetic parameter because of the increase of the resistive type drag force that has the tendency to reduce the motion of the nanofluids.

5. The motion of the nanofluid also decreases with the increases of thermal Grashof number. The increase of *Gr* increases the temperature of nanofluids, which governs to an increase in the upward buoyancy force. Therefore, the motion in nanofluids increases with increasing *Gr* because of the increment of buoyancy force.

Acknowledgements

Conflicts of interest

The authors declare that they have no conflicts of interest.

Nomenclature

Roman letters	
a, b	Constants depend on shape of nanoparticles
$\mathbf{B}_0$	Applied magnetic field
B_0	Magnitude of applied magnetic field
$\mathbf{B}$	Total magnetic field
b	Induced magnetic field
$(c_p)_s$	Heat capacity of solid nanoparticles
$(c_p)_f$	Heat capacity of base fluids

Roman letters

$(c_p)_{nf}$	Heat capacity of nanofluids
D	Rate of strain tensor
d_p	Diameter of solid nanoparticles
E	Total electric field
e	Internal energy per unit volume
exp	Exponential function
F	Force
f	Function of temperature and volume fraction, etc.
Gr	Thermal Grashof number
g	Gravitational acceleration
H(.)	Heaviside function
H	Total momentum of the system
I	Identity tensor
i	Cartesian unit vector in the x-direction
J	Current density
$\mathbf{J} \times \mathbf{B}$	Lorentz force
j	Cartesian unit vector in the y-direction
K	Dimensionless permeability parameter
k_s	Thermal conductivity of solid nanoparticles
k_f	Thermal conductivity of base fluids
k_{nf}	Thermal conductivity of nanofluids
k_b	Boltzmann constant
k	Cartesian unit vector in the z-direction
M	Magnetic parameter
m	Mass of the flow of fluids
N	Radiation parameter
Nu	Nusselt number
n	Empirical shape factors
p	Pressure
p_h	Hydrostatic pressure
p_d	Dynamic pressure
Pe	Peclet number
Q	Heat generation parameter
	Radiant flux vector
q_r	Magnitude of radiant heat flux
$\mathbf{q}''$	Heat conduction per unit area
q''	Magnitude of heat conduction per unit area

Roman letters	
Re	Reynolds number
r_c	Radius of gyration
S	Surface of the control volume
T	Cauchy stress tensor
T	Temperature
t	Time
u	Velocity in x-direction
U_0	Reference velocity
$\nabla\mathbf{V}$	Dyadic tensor
V	Velocity vector field
V	Control volume
V	Magnitude of velocity
v_0	Constant velocity in y-direction
W	Work done
Greek letters	
ρ_s	Density of solid nanoparticles
ρ_f	Density of base fluids
ρ_{nf}	Density of nanofluids
β_s	Volumetric coefficient of thermal expansion of solid nanoparticles
β_f	Volumetric coefficient of thermal expansion of base fluids.
β_{nf}	Volumetric coefficient of thermal expansion of nanofluids
μ_s	Dynamic viscosity of solid nanoparticles
μ_f	Dynamic viscosity of base fluids
μ_{nf}	Dynamic viscosity of solid nanofluids
β	Modeling function
φ	Volume fraction of solid nanoparticles
Ψ	Sphericity
ω	Oscillating parameter
ε	Perturbed parameter
λ	Williamson parameter
α_0	Mean absorption coefficient
σ_{nf}	Electrical conductivity of nanofluids
μ_m	Magnetic permeability
∇	Delta function
τ_1	Skin friction
τ	Viscous stress tensor

Author details

Aaiza Gul[1], Ilyas Khan[2]* and Sharidan Shafie[1]

*Address all correspondence to: ilyaskhanqau@yahoo.com

1 Department of Mathematical Sciences, Faculty of Science, Universiti Teknologi Malaysia, Skudai, Malaysia

2 Basic Engineering Sciences Department, College of Engineering Majmaah University, Majmaah, Saudi Arabia

References

[1] S. U. S. Choi, Enhancing thermal conductivity of fluids with nanoparticle, ASME FED, 66 (1995), 99–105.

[2] R. S. Vajjha and D.K. Das, Experimental determination of thermal conductivity of three nanofluids and development of new correlations, International Journal of Heat and Mass Transfer, 52 (2009), 4675–4682.

[3] M. T. Naik and L. S. Sundar, Investigation into thermophysical properties of glycol based CuO nanofluid for heat transfer applications, World Academy of Science Engineer Technology, 59 (2011), 440–446.

[4] S. Mansur, A. Ishak, and I. Pop, The magnetohydrodynamic stagnation point flow of a nanofluid over a stretching/shrinking sheet with suction, PLoS ONE, 10 (3) (2015), e0117733.

[5] E. V. Timofeeva, R. L. Jules, and S. Dileep, Particle shape effect on thermophysical properties of alumina nanofluids, Journal of Applied Physics, 106 (2009), 014304.

[6] P. Loganathan, P. N. Chand, and P. Ganesan, Radiation effects on an unsteady natural convection flow of a nanofluids past an infinite vertical plate, World Scientific Publishing Company, 8 (2013), 1350001–1350010.

[7] K. Asma, I. Khan, and S. Sharidan, Exact solutions for free convection flow of nanofluids with ramped wall temperature, The European Physical Journal Plus, 130 (2015), 57–71.

[8] S. Sebdani, M. Mahmoodi, and S. Hashemi, Effect of nanofluid variable properties on mixed convection in a square cavity, International Journal of Thermal Sciences, 52 (2012), 112–126.

[9] T. Fan, H. Xu, and I. Pop, Mixed convection heat transfer in horizontal channel filled with nanofluids, International Journal of Springer Plus, 34 (2013), 339–350.

[10] R. K. Tiwari and M. K. Das, Heat transfer augmentation in a two-sided lid-driven differentially heated square cavity utilizing nanofluids, International Journal of Heat and Mass Transfer, 50 (2007), 9–10.

[11] G. A. Sheikhzadeh, N. Hajialigol, M. E. Qomi, and A. Fattahi, Laminar mixed convection of Cu-water nano-fluid in two sided lid-driven enclosures, Journal of Nanostructures, 1 (2012), 44–53.

[12] S. Nadeem and S. Saleem, Unsteady mixed convection flow of nanofluid on a rotating cone with magnetic field, Apply Nanoscience, 4 (2014), 405–414.

[13] K. Al-Salem, H. F. Oztop, I. Pop, and Y. Varol, Effect of moving lid direction on MHD mixed convection in a linearly heated cavity, International Journal of Heat and Mass transfer, 55 (2012), 1103–1112.

[14] K. V. Prasad, K. Vajravelu, and P. S. Datti, The effect of variable fluid properties on the MHD flow and heat transfer over a non-linear stretching sheet, International Journal of Thermal Science, 49 (2010), 603–610.

[15] J. Y. Rami, A. Fawzi, and F. Abu-Al-Rub, Darcy-Forchheimer mixed convection heat and mass transfer in fluid saturated porous media, International Journal of Numerical Methods for Heat & Fluid Flow, 11 (2011), 600–618.

[16] T. Hayat, Z. Abbas, I. Pop, and S. Asghar, Effect of radiation and magnetic field on the mixed convection stagnation-point flow over a vertical stretching sheet in a porous medium, International Journal of Heat and Mass Transfer, 53 (2010), 466–474.

[17] R. L. Hamilton and O. K. Crosser, Thermal conductivity of heterogeneous two-component systems, Journal of Industrial & Engineering Chemistry Fundamentals, 1 (1962), 187–191.

[18] M. Turkyilmazoglu, Unsteady convection flow of some nanofluids past a moving vertical flat plate with heat transfer, Journal of Heat Transfer, 136 (2014), 031704–031711.

[19] A. Zeehan, R. Ellahi, and M. Hassan, Magnetohydrodynamic flow of water/ethylene glycol based nanofluids with natural convection through porous medium, European Physical Journal Plus, 129 (2014), 261.

[20] O. D. Makinde and P. Y. Mhone, Heat transfer to MHD oscillatory flow in a channel filled with porous medium, Romanian Journal of Physics, 50 (2005), 931–938.

[21] L. Colla, L. Fedele, M. Scattolini, and S. Bobbo, Water-based Fe_2O_3 nanofluid characterization: thermal conductivity and viscosity measurements and correlation, Advances in Mechanical Engineering, 2012 (Article ID 674947), 8.

[22] A. S. Noreen, M. Raza, and R. Ellahi, Influence of induced magnetic field and heat flux with the suspension of carbon nanotubes for the peristaltic flow in a permeable channel, Journal of Magnetism and Magnetic Materials, 381(2015), 405–415.

[23] R. Ellahi, S. Aziz, and A. Zeeshan, Non Newtonian nanofluids flow through a porous medium between two coaxial cylinders with heat transfer and variable viscosity, Journal of Porous Media, 16 (3) (2013), 205–216.

[24] A. S. Noreen, M. Raza, and R. Ellahi, Interaction of nanoparticles for the peristaltic flow in an asymmetric channel with the induced magnetic field, The European Physical Journal – Plus, 129 (2014), 155–167.

[25] M. Sheikholeslami and R. Ellahi, Three dimensional mesoscopic simulation of magnetic field effect on natural convection of nanofluid, International Journal of Heat and Mass Transfer, 89 (2015), 799–808.

[26] R. Ellahi, M. Hassan, and A. Zeeshan, Study on magnetohydrodynamic nanofluid by means of single and multi-walled carbon nanotubes suspended in a salt water solution, IEEE Transactions on Nanotechnology, 14 (4) (2015), 726–734.

[27] M. Sheikholeslami and R. Ellahi, Simulation of ferrofluid flow for magnetic drug targeting using Lattice Boltzmann method, Journal of Zeitschrift Fur Naturforschung A, Verlag der Zeitschrift für Naturforschung, 70 (2015), 115–124.

[28] M. Sheikholeslami, Effect of uniform suction on nanofluid flow and heat transfer over a cylinder, Journal of the Brazilian Society of Mechanical Sciences and Engineering, 37 (6) (2015), 1623–1633.

[29] R. Ellahi, M. Hassan, and A. Zeeshan, Shape effects of nanosize particles in Cu-H2O nanofluid on entropy generation, International Journal of Heat and Mass Transfer, 81 (2015), 449–456.

[30] M. Sheikholeslami, D. D. Ganji, M. Y. Javed, and R. Ellahi, Effect of thermal radiation on magnetohydrodynamics nanofluid flow and heat transfer by means of two phase model, Journal of Magnetism and Magnetic Materials, 374 (2015), 36–43.

[31] S. Rashidi, M. Dehghan, R. Ellahi, M. Riaz, and M. T. Jamal-Abad, Study of stream wise transverse magnetic fluid flow with heat transfer around an obstacle embedded in a porous medium, Journal of Magnetism and Magnetic Materials, 378 (2015), 128–137.

[32] S. A. Noreen, M. Raza, and R. Ellahi, Influence of heat generation and heat flux in peristalsis with interaction of nanoparticles, The European Physical Journal Plus, 129 (2014), 185.

[33] R. Ellahi, M. Hassan, and S. Soleimani, A study of natural convection heat transfer in a nanofluid filled enclosure with elliptic inner cylinder, International Journal for Numerical Methods for Heat and Fluid Flow, 24 (8) (2014), 1906–1927.

[34] M. Sheikholeslami, R. Ellahi, H. R. Ashorynejad, G. Domairry, and T. Hayat, Effects of heat transfer in flow of nanofluids over a permeable stretching wall in a porous medium, Computational and Theoretical Nanoscience, 11 (2) (2014), 486–496.

[35] M. SheikholeslamI, M. G. Bandpy, R. Ellahi, and A. Zeeshan, Simulation of CuO-water nanofluid flow and convective heat transfer considering Lorentz forces, Journal of Magnetism and Magnetic Materials, 369 (2014), 69–80.

[36] S. A. Noreen, S. U. Rahman, R. Ellahi, and S. Nadeem, Nano fluid flow in tapering stenosed arteries with permeable walls, International Journal of Thermal Sciences, 85 (2014), 54–61.

[37] R. Ellahi, The effects of MHD and temperature dependent viscosity on the flow of non-Newtonian nanofluid in a pipe: analytical solutions, Applied Mathematical Modeling, 37 (2013), 1451–1467.

[38] R. Ellahi, M. Raza, and K. Vafai, Series solutions of non-Newtonian nanofluids with Reynolds' model and Vogel's model by means of the homotopy analysis method, Mathematical and Computer Modelling, 55 (2012), 1876–1891.

[39] X. B. Wang, P. L. Zhou, and F. X. Peng, A fractal model for predicting the effective thermal conductivity of liquid with suspension of nanoparticles, International Journal of Heat and Mass Transfer, 46 (14) (2003), 2665–2672.

[40] M. Abareshi, E. K. Goharshadi, S. M. Zebarjad, H. K. Fadafan, and A. Youssefi, Fabrication, characterization and measurement of thermal conductivity of Fe_3O_4 nanofluids, Journal of Magnetism and Magnetic Materials, 322(24) (2010), 3895–3901.

[41] S. E. Borglin, G. J. Moridis, and C. M. Oldenburg, Experimental studies of the flow of ferrofluid in porous media, Transport in Porous Media, 41 (1) (2000), 61–80.

[42] M. Sheikholeslami, N. S. Akbar, and M. T. Mustafa, MHD effect on nanofluid with energy and hydrothermal behavior between two collateral plates: application of new semi analytical technique, Thermal Science, (2015), 95–95. doi:10.2298/TSCI150228095S.

[43] M. Sheikholeslami, K. Vajravelu, and M. M. Rashidi, Forced convection heat transfer in a semi annulus under the influence of a variable magnetic field, International Journal of Heat and Mass Transfer, 92 (2016), 339–348.

[44] M. Sheikholeslami and M. M Rashid, Non-uniform magnetic field effect on nanofluid hydrothermal treatment considering Brownian motion and thermophoresis effects, Journal of the Brazilian Society of Mechanical Sciences and Engineering, 38 (4) (2016), 1171–1184.

[45] M. Sheikholeslami, M. M. Rashidi, and D. D. Ganji, Effect of non-uniform magnetic field on forced convection heat transfer of water nanofluid, Computer Methods in Applied Mechanics and Engineering, 294 (2015), 299–312.

[46] M. Sheikholeslami and M. M. Rashidi, Ferrofluid heat transfer treatment in the presence of variable magnetic field, The European Physical Journal Plus, 130 (6) (2015), 1–12.

[47] M. Sheikholeslami and S. Abelman, Two-Phase simulation of nanofluid flow and heat transfer in an annulus in the presence of an axial magnetic field, IEEE Transactions on Nanotechnology, 14 (3) (2015), 561–569.

[48] M. Sheikholeslami and A. J. Chamkha, Flow and convective heat transfer of a ferro-nanofluid in a double-sided lid-driven cavity with a wavy wall in the presence of a variable magnetic field, Numerical Heat Transfer, Part A: Applications 69 (10) (2016), 1186–1200.

[49] M. Sheikholeslami, M. M. Rashidi, T. Hayat, and D. D. Ganji, Free convection of magnetic nanofluid considering MFD viscosity effect, Journal of Molecular Liquids, 218 (2016), 393–399.

[50] M. Sheikholeslami, M. G. Bandpy, R. Ellahi, M. Hassan, and S. Soleimani, Effects of MHD on Cu–water nanofluid flow and heat transfer by means of CVFEM, Journal of Magnetism and Magnetic Materials, 349 (2014), 188–200.